Alexandre Sze, S. Mehdi Belgnaoui, David Olagnier, Rongtuan Lin, John Hiscott, and Julien van Grevenynghe

Host restriction factor SAMHD1 limits Human T-cell Leukemia Virus Type 1 (HTLV-1) infection of monocytes through STING-mediated apoptosis

Published in:
Cell Host & Microbe14.4 (October 16, 2013): 422-434

doi: 10.1016/j.chom.2013.09.009
http://www.cell.com/cell-host-microbe/abstract/S1931-3128(13)00329-6

Host restriction factor SAMHD1 limits Human T-cell Leukemia Virus Type 1 (HTLV-1) infection of monocytes through STING-mediated apoptosis

Alexandre Sze[1], S. Mehdi Belgnaoui[1], David Olagnier[2], Rongtuan Lin[1], John Hiscott[1,2*], and Julien van Grevenynghe[1,2*]

[1]Lady Davis Institute-Jewish General Hospital, McGill University, Montreal, Canada H3T 1E2

[2]Vaccine and Gene Therapy Institute of Florida, Port St. Lucie, Fl. 34987, United States

[*]Correspondence: julien.vangrevenynghe@mail.mcgill.ca; Tel:514-340-8222 ext#5265 (JvG.); jhiscott@vgtifl.org, Tel:772-345-5694 (JH.)

Running title: SAMHD1 blocks HTLV-1 infection via STING

SUMMARY

Human T-cell leukemia virus type 1 (HTLV-1) is the causative agent of adult T cell leukemia and HTLV-1-associated myelopathies. HTLV-1 virions are poorly infectious and do not stably infect $CD4^+$ T lymphocytes; however, HTLV-1 does efficiently infect cells of the myeloid lineage. Here, we investigate the mechanisms underlying monocyte depletion driven by HTLV-1 infection, and demonstrate that exposure of monocytes to HTLV-1 results in an abortive infection, accompanied by apoptosis that is dependent on the host restriction factor SAMHD1. Reverse transcription intermediates (RTI), produced in the presence of SAMHD1, induced IRF3-mediated antiviral and apoptotic responses. The viral RTI complexed with the DNA sensor STING, resulting in the formation of a pro-apoptotic IRF3-Bax complex leading to apoptosis. Overall, this study provides a mechanistic explanation for abortive retroviral infection of monocytes and reports a link between SAMHD1 restriction, sensing of retroviral HTLV-1 RTI by STING, and initiation of IRF3-Bax driven apoptosis.

HIGHLIGHTS

HTLV-1 elicits a non-productive infection and an antiviral response in primary human monocytes.

Host restriction factor SAMHD1 prevents synthesis of viral DNA and mediates mitochondrial dependent apoptosis.

HTLV-1 reverse transcription intermediates (RTI) complex with the DNA sensor STING and trigger apoptosis.

RTI and STING interaction generates an IRF3-Bax complex that triggers apoptosis and limits HTLV-1 infection.

INTRODUCTION

Infection with human T-cell leukemia virus type 1 (HTLV-1) affects approximately 20 million people worldwide (Cook et al., 2013), and is a major cause of mortality and morbidity in endemic areas such as southern Japan, the Caribbean basin, Central/South America, and Western Africa (Ragin et al., 2008). Although most of the infected individuals are asymptomatic carriers of the virus, they are also at risk for opportunistic infections (Verdonck et al., 2007). In addition, chronic infection with HTLV-1 can lead to a number of severe pathologies associated with poor prognosis, including the aggressive and fatal adult T-cell leukemia (ATL), progressive HTLV-1-associated myelopathy/tropical spastic paraparesis (HAM/TSP), uveitis and infective dermatitis in children (Cook et al., 2013; Yamano and Sato, 2012). HTLV-1 has a preferential tropism for $CD4^+$ T-cells in asymptomatic carriers and ATL patients, while both $CD4^+$ and $CD8^+$ T-cells constitute viral reservoirs in HAM/TSP patients (Cook et al., 2013). Unlike most retroviruses, cell-free HTLV-1 is poorly infectious and does not stably infect its primary $CD4^+$ T lymphocyte target. Rather, HTLV-1 utilizes various cell-to cell transmission strategies, including transfer of viral assemblies, formation of virological synapses, or formation of intracellular conduits (Igakura et al., 2003; Pais-Correia et al., 2010; Van Prooyen et al., 2010). HTLV-1 also infects cells of the myeloid lineage, which play critical roles in the host innate response to viral infection. For instance, previous studies have shown that cell-free HTLV-1 particles can productively infect DC, which then participate in viral transmission to and transformation of $CD4^+$ T-cells (Jones et al., 2008). HTLV-1 infection of DC elicits early antiviral responses that are mediated by the production of type I interferon (IFN) (Colisson et al., 2010), although the number of peripheral DC as well as the IFN response are markedly reduced in chronically infected asymptomatic and ATL subjects (Hishizawa et al., 2004). Monocyte precursors that would normally replenish the DC population are unable to properly differentiate during chronic

HTLV-1 infection and recent evidence indicates monocyte depletion in HTLV-1 infected patients (Makino et al., 2000; Nascimento et al., 2011). The molecular consequences of *de novo* HTLV-1 infection on host innate immunity in monocytic cells have yet to be elucidated.

Human myeloid and bystander $CD4^+$ T-cells are refractory to HIV-1 infection, in part because the host restriction factor SAMHD1 prevents efficient viral DNA synthesis (Baldauf et al., 2012; Descours et al., 2012; Laguette and Benkirane, 2012; Laguette et al., 2011). SAMHD1 functions within non-dividing cells as a deoxynucleoside triphosphate triphosphohydrolase, which hydrolyzes the endogenous pool of deoxynucleoside triphosphates (dNTP) to levels below the threshold required for reverse transcription (Ayinde et al., 2012; Goldstone et al., 2011; Lahouassa et al., 2012). SAMHD1 was initially characterized in the context of the autoimmune disorder Aicardi-Goutières syndrome, and genetic mutations that render SAMHD1 non-functional result in uncontrolled inflammatory and type I IFN responses against self DNA (Rice et al., 2009). Primary cells from these patients are highly susceptible to HIV-1 infection (Baldauf et al., 2012; Berger et al., 2011; Descours et al., 2012). The Vpx accessory protein of HIV-2 and its counterpart in certain strains of SIV antagonize SAMHD-1 by inducing proteasome-dependent degradation (Ayinde et al., 2012; Laguette et al., 2012). HIV-1 restriction mediated by SAMHD-1 is overcome by silencing its expression with Vpx, or by the addition of exogenous dN (deoxynucleosides) (Baldauf et al., 2012; Descours et al., 2012; Laguette et al., 2011; Lahouassa et al., 2012).

Recognition of evolutionarily conserved molecular structures shared by pathogens, known as pathogen-associated molecular patterns (PAMP), is critical for the initiation of innate immune responses (Kumar et al., 2011). Multiple surface and cytosolic pathogen recognition receptors (PRR) (Kawai and Akira, 2011) have now been identified that sense and respond to microbial

infection. Toll-like receptors (TLR) detect distinct PAMP such as lipopolysaccharide (TLR4), single and double stranded RNA (TLR7/8 and TLR3, respectively) and CpG DNA (TLR9) (Blasius and Beutler, 2010; Kawai and Akira, 2011). The retinoic acid-inducible gene-I (RIG-I)-like receptors (RLR) - which include RIG-I and MDA5 - represent another PRR family that recognises cytosolic viral RNA (Blasius and Beutler, 2010; Kawai and Akira, 2011). PRR responsible for the detection of cytosolic DNA include DAI, DDX41, cGAS and IFI16 - all of which trigger IFN production - as well as AIM2 that stimulates an inflammasome dependent-secretion of the pro-inflammatory IL-1β cytokine (Barber, 2011; Sun et al., 2013). The endoplasmic reticulum resident adapter STING functions as a DNA sensor for bacterial cyclic GTP (Burdette and Vance, 2013) and mediates detection of viral DNA (Ishikawa and Barber, 2008; Ishikawa et al., 2009; Zhong et al., 2008). STING can also directly complex with single stranded (ss) and double stranded (ds) cytoplasmic viral DNA to initiate antiviral signalling (Abe et al., 2013).

In the present study, we characterized *de novo* infection of primary human monocytes by HTLV-1 and demonstrated that HTLV-1 infection induces SAMHD1-mediated apoptosis in monocytic cells. We further showed that production of HTLV-1 reverse transcription intermediates (RTI), generated in the presence of SAMHD-1, complexed with the innate immune sensor STING and initiated IRF3-Bax directed apoptosis. These results elucidate for the first time the mechanism of HTLV-1 abortive infection of monocytes and link the host restriction factor SAMHD1, the sensing of retroviral RTI by STING, and the initiation of IRF3-Bax-driven apoptosis.

RESULTS

Abortive infection of primary monocytes by HTLV-1 activates type I IFN response. To characterize the impact of HTLV-1 infection on the activation of the host antiviral response in primary human monocytes, we first assessed the percentage of HTLV-1 infected monocytes at 3h post-infection (pi), using increasing concentrations of purified HTLV-1 (0-5 μg/mL). Virus binding to monocytes was dependent on the quantity of HTLV-1, as illustrated by surface staining with anti-Env (gp46) monoclonal antibodies (**Figure 1A**); for subsequent experiments, an HTLV-1 concentration of 2μg/ml was used, since >90% of the cells displayed virus binding (**Figure 1A**) (91.7 ± 4.8% $gp46^+$cells; $P > 0.05$; n = 5). HTLV-1 particles were efficiently internalized by monocytes, as demonstrated by the detection of intracellular HTLV-1 viral RNA (vRNA) starting at 3h pi, with the viral RNA load gradually decreasing over the 120h time course (**Figure 1B**). HTLV-1 internalization in monocytes was further demonstrated by intracellular staining (ICS) for the viral matrix protein p19 at 24h pi (**Figure 1C**, blue histograms) (86.7 ± 6.2% of $p19^+$ monocytes; $P < 0.01$ compared to uninfected cells; n = 5). Importantly, viral binding and internalization was eliminated by pre-treating HTLV-1 with anti-gp46 neutralizing mAb or pre-treating monocytes with 0.1% trypsin (Jones et al., 2005) (**Figure 1C**) ($P < 0.01$ compared to infected cells). The absence of intracellular Tax protein and virion release at 24 and 48h pi indicated that monocytes were not productively infected by HTLV-1 (**Figure 1C** and **Figure S1** respectively). Monocyte-derived DC (MDDC), on the other hand, were productively infected with HTLV-1 (40.6 ± 5.7% Tax^+ cells at 24h pi) (data not shown).

Despite the non-productive infection by HTLV-1, monocytes generated a robust innate immune response, as illustrated by the induction of multiple parameters of the antiviral signaling pathway. An early increase in phosphorylated interferon regulatory factor 3 (P-IRF3) was

detected at 3h pi (**Figure 1D**), while increased expression of STAT1, phosphorylated STAT1 (P-STAT1), interferon stimulated gene 56 (ISG56) and RIG-I were observed at 24 and 48h pi.

HTLV-1-infected monocytes undergo apoptosis. To further pursue the fate of HTLV-1-infected monocytes, we next evaluated the level of apoptosis in HTLV-1-infected $CD3^{-}CD14^{+}$ monocytes at 3-120h pi by Annexin-V staining. At 24h pi, infected monocytes displayed higher levels of apoptosis than uninfected cultures (**Figure 2A**) (22.9 ± 3.5% versus 8.6 ± 1.3%, respectively; $P < 0.01$; n = 5), and by 72h the percentage of HTLV-1 infected apoptotic cells increased to over 45%. Infection of monocytes with a low dose of HTLV-1 (0.1 μg/ml) also resulted in the induction of apoptosis in the $p19^{+}$population (**Figure S2A**). We did not observe induction of necrosis, or an effect of necrostatin-1 treatment on infected monocytes at 48h pi (**Figure S3A**). Apoptosis was accompanied by the generation of cleaved caspase-3 ($_{CL}$caspase-3) in infected cells (**Figure 2B** and **Figure S2B**) (33.4 ± 12.3% and 11.4 ± 2%, respectively for HTLV-1-infected and uninfected cells at 48h pi; $P < 0.01$; n = 5); infected cells also exhibited a loss of mitochondrial potential as shown by reduced $DiOC_6(3)$ intensity when compared to uninfected cells (**Figure 2C** and **Figure S2C**) ($P < 0.01$; n = 5). The pan-caspase inhibitor ZVAD or the blocking α-gp46 mAb prevented $_{CL}$caspase-3-mediated apoptosis (**Figure 2B**) and mitochondrial depolarization (**Figure 2C**). Treatment with ZVAD however did not interfere with the internalization of HTLV-1, as detected by measuring intracellular p19 (**Figure 2B**, blue histograms) ($P > 0.05$; n = 5). A strong statistical correlation between (*i*) caspase-3 activation, (*ii*) mitochondrial depolarization and apoptosis was confirmed by the non-parametric Spearman test (**Figure 2D**) (r = 0.7845 and 0.9036, respectively for (*i*) and (*ii*); $P < 0.0001$; n = 25). Expression of mitochondrial pro- and anti- apoptotic molecules were also analyzed; increased Bax expression and caspase-9 cleavage were observed in infected monocytes (**Figure 2E**) ($P <$

0.05 and $P < 0.01$ respectively; n = 3), while expression of Bcl-2 family members - Bim, Noxa, Bcl-2, and Mcl-1 - were unchanged. An increased expression of cleaved caspase-1 at 30 min and bioactive IL-1β at 3h pi was detected after HTLV-1 infection, indicating the activation of the inflammasome (**Figure S3B**). To investigate caspase-1-associated pyroptosis, HTLV-1-infected cells were treated with Ac-YVAD-cmk (YVAD; a selective inhibitor of caspase-1); a minor, but significant, improvement of cell survival was observed (**Figure S3C**).

A requirement for SAMHD1 in HTLV-1-driven apoptosis in infected monocytes. The above observations, detailing abortive HTLV-1 infection of monocytes are reminiscent of the functional consequences of host restriction by SAMHD1 during HIV-1 infection (Baldauf et al., 2012; Descours et al., 2012; Doitsh et al., 2010; Laguette et al., 2011), prompting us to investigate whether SAMHD1 functioned similarly to restrict HTLV-1 infection. Small interfering RNA (siRNA)-mediated silencing of SAMHD1 in primary monocytes resulted in a 72 ± 11.8% reduction in protein expression (**Figure 3A**). SAMHD1 silencing did not alter HTLV-1 internalization in monocytes at 48h pi - 95.5 ± 1% and 94.2 ± 3.1% [% of $p19^{+}$monocytes] -, respectively for control and SAMHD1-specific siRNA-transfected monocytes (**Figure 3B**, **right histograms**). Following HTLV-1 infection, induced apoptosis was also reduced by ~70% in SAMHD1-silenced monocytes compared to control siRNA-treated monocytes (**Figure 3B**) ($P < 0.01$; n = 5). The correlation between inhibition of SAMHD1 expression and inhibition of HTLV-1-induced apoptosis in primary monocytes was significant (**Figure 3C**) ($r = 1$; $P = 0.0167$; n = 5, Spearman test).

The deoxynucleoside triphosphate triphosphohydrolase function of SAMHD1 has been shown to block reverse transcription of retroviral DNA by depleting the dNTP pool required for complete reverse transcription (Ayinde et al., 2012; Goldstone et al., 2011; Hollenbaugh et al.,

2013; Kim et al., 2012; Lahouassa et al., 2012), an effect that is reversed by the addition of exogenous dN (Lahouassa et al., 2012). To explore the relationship between the triphosphohydrolase activity of SAMHD1 and induced apoptosis, primary monocytes were infected with HTLV-1 in the presence of increasing concentrations of exogenous dN (0-100nM). SAMHD1-mediated apoptosis was inhibited by the addition of exogenous dN in a dose-dependent manner (**Figure 3D**), with apoptosis reduced to control levels in monocytes treated with 100nM dN (> 80% inhibition of apoptosis). We did not observe *de novo* Tax expression following SAMHD1 knockdown or dN treatment in infected monocytes at 48h pi (n = 3; data not shown). These results demonstrate that nucleotide pool depletion, mediated by SAMHD1 function, correlates directly with HTLV-1-induced apoptosis.

HTLV-1-induced apoptosis correlates with the generation of cytosolic RTI. Previous studies in the context of HIV-1 infection demonstrated that incomplete cytoplasmic DNA triggered a pro-apoptotic response in infected bystander $CD4^+$ T-cells (Doitsh et al., 2010). To assess the presence of reverse transcription intermediates (RTI) in HTLV-1-infected monocytes, viral DNA was measured in total versus nuclear fractions by qPCR at 3-120h pi; HTLV-1 RTI were detected only in the total fraction (**Figure 4A** and **Figures S4A, B**), indicating that viral DNA synthesis was initiated in the cytosol, but was not fully reverse transcribed and did not reach the nucleus. As previously reported, the presence nuclear retroviral DNA implies the completion of reverse transcription and the formation of the pre-integration complex (Nisole and Saib, 2004). Silencing SAMHD1 expression or treatment with exogenous dN led to the detection of HTLV-1 DNA in the nucleus, as well as integrated provirus, in infected monocytes (**Figure 4B** and **Figure S4C**).

Several primer pairs were designed to monitor sequential steps in HTLV-1 reverse transcription, including the initial generation of strong-stop DNA (*5´utr*), and DNA elongation (*env* or *gag*) (**Figure 4C, upper schematic** and **Table S1**) (Doitsh et al., 2010). Primary monocytes were treated with 5μM azidothymidine (AZT), a nucleoside analog reverse transcriptase inhibitor that prevents elongation of reverse transcribed DNA after initiation (Doitsh et al., 2010), and then infected with HTLV-1. AZT treatment had no inhibitory effect on the initiation of HTLV-1 reverse transcription (**Figure 4C**), as detected with the *5'utr* primers (green), whereas DNA strand elongation was progressively inhibited, as detected using *env* (blue) and *gag* (orange) region specific probes (**Figure 4C**) (35.5 ± 31.3% and 65.5 ± 22.7% inhibition respectively; $P < 0.01$; n = 5). Following HTLV-1 infection, apoptosis in monocytes treated with AZT was reduced by >40% compared to infected cells without AZT (**Figure 4D**) (41.8 ± 12.3%; $P < 0.05$; n = 5). Treatments with dN or AZT did not reduce apoptosis during etoposide treatment, a nonspecific apoptotic inducer, excluding their potential pro-survival side-effects (**Figure S2D**). These results demonstrate that AZT blocked HTLV-1 DNA elongation and suggested that cytosolic RTI generation was linked with virus-mediated apoptosis.

These primers were also used in the context of SAMHD1 silencing, to investigate the production of early versus late stage RTI. SAMHD1 knockdown led to a decrease in the generation of total and early transcripts (green [*5´utr*]; 1.45 ± 0.41 fold decrease), concomitant with an accumulation of late reverse transcription products (orange [*gag*]; 1.39 ± 0.27 fold increase) (**Figure 4E**). This panel indicates that during SAMHD1 silencing, the number of times reverse transcription is re-initiated is reduced, resulting in an overall decrease in the RTI load.

To confirm if HTLV-1 replicative intermediates directly mediated apoptosis, synthetic single (ss) or double stranded (ds) 90 nucleotide HTLV-1 DNA (vDNA) - conjugated with biotin - were

introduced into primary monocytes. Monocytes harboring HTLV-1 ss or $dsDNA_{90}$ ($vDNA^+$cells; green histograms) underwent apoptosis (59.2 ± 3.5% and 48.9 ± 6.9% respectively), whereas vDNA-free monocytes from the same samples did not undergo apoptosis (purple histograms; ~30% apoptosis in cells electroporated only, or transfected with digested $ssDNA_{90}$ (data not shown) (**Figure 4E**). The transfection of monocytes with scrambled RTI (whose sequence was generated by randomizing the U5 sequence) did not result in the induction of apoptosis, confirming the specificity of HTLV-1 RTI to induce apoptosis (**Figure 4F**). Overall, these results provide evidence for the direct contribution of cytosolic RTI during HTLV-1-induced apoptosis.

HTLV-1 RTI signals via STING to induce apoptosis and the IFN response. The endoplasmic reticulum resident transmembrane sensor STING (stimulator of interferon genes) is central to the generation of an innate immune response, through its capacity to directly bind viral and bacterial DNA (Abe et al., 2013; Burdette and Vance, 2013; Ishikawa and Barber, 2008; Ishikawa et al., 2009). Given the importance of STING in initiating cytoplasmic DNA signaling events, we next examined whether STING could recognize and complex with HTLV-1 RTI. Using streptavidin beads to pull-down biotinylated HTLV-1 DNA, we demonstrated that STING was precipitated from primary monocytes via interactions with ss or $dsDNA_{90}$ (**Figure 5A).** Furthermore, the formation of the complex between STING and HTLV-1 DNA was associated with the induction of type I IFN signalling and apoptosis, as illustrated by increased expression of RIG-I, ISG56 and Bax (**Figure 5A**) ($P < 0.01$; n = 3). Transfection of monocytes with scrambled RTI resulted in STING pull-down and the induction of ISGs. However, no increase in Bax expression was observed in these cells. No complex formation was observed between HTLV-1 RTI and the RNA sensor RIG-I (**Figure 5A**).

To determine whether cytosolic detection of HTLV-1 RTI by STING was involved in triggering apoptosis, STING-specific siRNA was introduced into primary monocytes, resulting in ~65% inhibition of STING expression (**Figure 5B**) ($P < 0.01$; n = 5). Knockdown of STING in primary monocytes resulted in a significant improvement in cell survival. In multiple experiments, a 55-60% inhibition of apoptosis was observed (**Figure 5C and Figure S5**) ($P < 0.01$ compared to control siRNA-treated cells; n = 5). A positive correlation between the inhibition of STING expression and HTLV-1-induced apoptosis was established using the non-parametric Spearman test (**Figure 5D**) ($r = 1$; $P = 0.0167$; n = 5). Altogether, these results indicate that HTLV-1 RTI, generated in primary monocytes in a SAMHD1-dependent manner, complex with the DNA sensor STING and initiate apoptosis.

HTLV-1 RTI triggers mitochondrial apoptosis through IRF3-Bax signalling. HTLV-1 infection of monocytes stimulated IRF3 activation and induction of pro-apoptotic Bax (**Figures 1D** and **2E**), suggesting that HTLV-1 may trigger apoptosis via a mechanism involving the formation of a pro-apoptotic complex between IRF3 and Bax (Chattopadhyay et al., 2010; Chattopadhyay et al., 2011). To determine whether STING recognition of HTLV-1 RTI could trigger apoptosis through IRF3-Bax signalling, we measured Bax and ISG expression, as well as IRF3 phosphorylation in infected monocytes knocked down for STING expression. By immunoblot analysis, all parameters - Bax, P-IRF3, RIG-I and ISG56 expression - were inhibited 95.1 ± 8.5%, 72.1 ± 13.3%, 66.2 ± 48% and 64.5 ± 29.3% respectively by STING knockdown ($P < 0.01$ compared to infected cells treated with control siRNA; n = 3) (**Figure 6A**), thus supporting a role for STING in regulating both the antiviral and apoptotic responses. Similarly, we observed a 73 ± 15.8% inhibition of Bax-expressing monocytes when STING was silenced (**Figure S6**). As with *de novo* HTLV-1 infection, the addition of cytosolic ss or $dsDNA_{90}$ led to

increased Bax expression (**Figure 6B**, **input blots**) ($P < 0.05$; n = 3). Strikingly, both HTLV-1 infection and the addition of biotinylated ss or $dsDNA_{90}$ resulted in the generation of a complex between IRF3 and Bax (**Figure 6B**), whereas no IRF3-Bax complex was observed in monocytes transfected with scrambled RTI. The formation of this pro-apoptotic complex required both SAMHD1 and STING expression, since RNAi-mediated silencing of either target not only decreased Bax expression, but also abrogated physical association between IRF3 and Bax (**Figure 6C**).

To pursue the involvement of Bax in the apoptosis mediated by HTLV-1 infection, a multi-parametric antibody cocktail was generated to measure the levels of Annexin-V, Bax and $DiOC_6(3)$ co-staining on gated $CD14^+$monocytes. Infected monocytes expressing Bax (red subset) displayed higher levels of mitochondria depolarization and Annexin-V co-staining, compared to the green Bax^{neg} cells (**Figure 6D**) (74.3 ± 24.8% and 34.3 ± 5.9% $DiOC_6(3)^{low}$ Annexin-V^+ cells, respectively; $P < 0.01$; n = 5). Furthermore, siRNA-mediated silencing of Bax expression reduced the level of apoptosis by ~60%, thus confirming the involvement of Bax in HTLV-1 driven monocyte cell killing (**Figure 6E**).

HIV-1 DNA recognition by STING induces a pro-apoptotic response. Finally, we next examined whether STING-mediated recognition of RTI corresponding to strong-stop HIV-1 DNA also led to monocyte depletion through IRF3-Bax driven apoptosis. HIV-1 $ssDNA_{90}$ RTI was introduced into primary monocytes for 3h; IRF3 phosphorylation and Bax expression were increased ~7-10 fold with the HIV-1 RTI (**Figure 7A**) ($P = 0.0053$ and $P = 0.0115$ respectively, compared to RTI-free monocytes; n = 3). Importantly, using streptavidin beads to precipitate biotinylated HIV-1 $ssDNA_{90}$, STING, but not RIG-I, was also readily pulled-down in association with HIV RTI (**Figure 7B**). As with HTLV-1, the addition of biotinylated HIV-1 $ssDNA_{90}$

resulted in the generation of a heterodimeric IRF3-Bax complex (**Figure 7C**). Furthermore, monocytes transfected 48h with HIV-1 RTI also displayed significantly higher levels of mitochondria-dependent apoptosis (**Figure 7D**). Overall, these data demonstrate that retroviral RTI recognition by STING induces mitochondria-dependent apoptosis via the formation of the pro-apoptotic IRF3-Bax heterodimer (**Figure S7**).

DISCUSSION

In this study, we demonstrate that *de novo* HTLV-1 infection initiates an abortive infection of primary monocytes and triggers mitochondrial depolarization and caspase-3 dependent cell death. HTLV-1 infection also stimulated induction of a type I IFN response, mediated through IRF3 activation and triggering of Jak-STAT1 signaling. HTLV-1-induced apoptosis in monocytes was dependent on the triphosphohydrolase activity of SAMHD1, since silencing its expression, or the introduction of exogenous dN in HTLV-1-infected monocytes significantly reduced apoptosis. HTLV-1 reverse transcription intermediates (RTI) were detected exclusively in the cytoplasm of infected monocytes from 3-120h post-infection, and it was only after inhibition of SAMHD1 expression that HTLV-1 DNA was detected in the nucleus compartment. The continued presence of RTI in the cytoplasm was sensed by the ER resident DNA sensor STING. Because of the involvement of STING in activation of the type I IFN response, we examined the fate of IRF3 and detected the formation of an IRF3-Bax complex, which was responsible for the mitochondrial depolarization and apoptosis. These experiments provide a mechanistic explanation for abortive retroviral infection of monocytes and establish a link between SAMHD1 restriction, sensing of retroviral RTI by STING, and the initiation of IRF3-Bax induced apoptosis. The scope of these observations was further extended by the

demonstration that HIV-1 RTI also complexed with STING and triggered apoptosis in the same manner (summarized in **Figure S7**).

The analogy between the current results and restriction of HIV-1 by SAMHD1 is striking, and a number of recent studies have detailed the capacity of SAMHD1 to limit HIV-1 replication in quiescent $CD4^+$ T-cells and myeloid cells (Baldauf et al., 2012; Descours et al., 2012; Laguette and Benkirane, 2012; Laguette et al., 2011). Prior to the characterization of the role of SAMHD1, Doitsh *et al.* had demonstrated that abortive HIV-1 reverse transcription in resting tonsil $CD4^+$ T cells resulted in apoptotic cell death, triggered by the accumulation of incomplete HIV-1 reverse transcripts (Doitsh et al., 2010). It has since become clear that SAMHD1 is involved in restricting HIV-1 reverse transcription through its dNTP triphosphohydrolase activity, which depletes the intracellular pool of dNTP (Ayinde et al., 2012; Goldstone et al., 2011; Lahouassa et al., 2012). The intracellular dNTP pool appears to be an important rate-limiting factor for retroviral reverse transcription, and SAMHD1 critically modulates this process. SAMHD1 is highly active in monocytes that have low levels of intracellular dNTP (Kaushik et al., 2009; Triques and Stevenson, 2004). In the presence of SAMHD1, nuclear or integrated HTLV-1 DNA was never detected in infected monocytes, whereas SAMHD1 silencing or restoration of the dNTP pool resulted in the inhibition of virus-induced apoptosis, as well as the completion of vDNA synthesis and translocation into the nucleus. Similarly, reduction of cytoplasmic HTLV-1 RTI levels by administration of AZT also improved cell viability. To investigate directly a role for RTI in triggering apoptosis, a biotinylated 90 nucleotide single or double stranded RTI from the U5 region of HTLV-1 was introduced into monocytes and it triggered apoptosis in a manner similar to infection.

One of the outstanding questions raised by these cumulative studies is: how does SAMHD1-mediated restriction of retroviral replication initiate apoptosis and impact the host innate response to retroviral infection? Our experiments provide evidence that the endoplasmic reticulum resident adapter STING triggers both processes through IRF3 activation. STING is known to regulate type I IFN immunity following recognition of pathogen DNA (Ishikawa et al., 2009); its ability to directly interact with viral DNA was characterized recently and STING was shown to be the primary sensor involved in DNA recognition (Abe et al., 2013). Although STING was readily pulled down in biotin-streptavidin complexes with RTI, we cannot formally exclude the involvement of other DNA sensors such as MRE11 (Kondo et al., 2013), DDX41 (Zhang et al., 2011), IFI16 (Unterholzner et al., 2010), or cGAS (Sun et al., 2013) in the recognition of retroviral RTI. The release of type 1 IFN and/or pro-inflammatory cytokines during HTLV-1 infection could also contribute to the induction of apoptosis in monocytes.

Complex formation between STING and HTLV-1 RTI initiated apoptosis through the formation of an IRF3-Bax complex, a novel apoptotic mechanism involved in the clearance of virus-infected cells via activation of effector caspase-3 (Chattopadhyay et al., 2013; Chattopadhyay et al., 2010).. Following HTLV-1 infection of monocytes, we detected IRF3-Bax complex formation at 3h pi, prior the induction of RIG-I expression, and complex formation was abrogated in monocytes when STING expression was silenced, thus identifying STING signaling as an additional pathway involved in IRF3-Bax induction. We did not observe a requirement for RIG-I during HTLV-1-induced apoptosis or RIG-I involvement in IRF3-Bax formation; no interaction was observed between RTI and RIG-I, and silencing RIG-I had no effect on HTLV-1-induced apoptosis (**Figures S5A, B**). That IRF3 activation can promote both apoptotic and antiviral signalling was also demonstrated in earlier studies in which constitutively active forms

of IRF3 and IRF7 were transduced into primary macrophages (Goubau et al., 2009). Transcriptional profiling and biological characterization of transduced human macrophages demonstrated that IRF3 initiated an antiviral response, but also rapidly induced cell death through the up-regulation of a subset of pro-apoptotic genes (Goubau et al., 2009).

We observed similar apoptotic mechanisms associated with STING binding and IRF3-Bax induction of apoptosis when HIV-1 RTI were introduced into monocytes, arguing in favour of the generality of the SAMHD1-STING initiation of apoptotic signaling in human retroviral infection **(Figure 7).** This observation, however, is not applicable in the context of HIV-2 which expresses Vpx; the physical interaction of SAMHD1 with Vpx recruits the Cul4-DDB1-DCAF1 complex to drive its proteasomal degradation (Descours et al., 2012; Laguette et al., 2011; Lahouassa et al., 2012). Furthermore, the exonuclease TREX1 suppresses recognition of HIV-1 replicative intermediates by STING as a viral evasion mechanism (Yan et al., 2010).

No correlation was observed between HTLV-1-induced apoptosis and expression levels of SAMHD1 (data not shown), consistent with Descours *et al.* who demonstrated that HIV-1 restriction was not solely associated with SAMHD1 expression levels (Descours et al., 2012). In fact, monocyte-derived DC are productively infected by HTLV-1 (Abe et al., 2013; Jones et al., 2008), despite SAMHD1 expression (Laguette et al., 2011). Moreover, in macrophages and cycling $CD4^+$ T-cells, HTLV-1 infection was not blocked by SAMHD1 and led to Tax production (Gramberg et al., 2013), indicating that SAMHD1 function differs in other cell contexts. It is likely that regulation of SAMHD1 restriction depends on several retroviral and host parameters including post-translational modifications, cellular co-factors, and splice variations (Descours et al., 2012; Welbourn et al., 2012). In this regard, it was recently

demonstrated that SAMHD1 activity is modulated by phosphorylation status. Cyclin A2/CDK1 phosphorylated SAMHD1 at Thr592 SAMHD1 in cycling cells, and phosphorylation at Thr592 correlated with loss of restriction (Cribier et al., 2013; White et al., 2013). Furthermore, type 1 IFN treatment reduced Thr592 phosphorylation, indicating a link between SAMHD1 phosphorylation, antiviral activity and innate immune signaling(Cribier et al., 2013). White *et al.* further demonstrated that T592 phosphomimetic SAMHD1 mutants did not restrict HIV-1 replication, despite dNTPase activity, oligomer formation, and nuclear localization(White et al., 2013). These experiments identify phosphorylation of SAMHD1 at Thr592 by cyclin A2/CDK1 as an important regulatory mechanism, and highlight the need for further studies to elucidate the mechanisms that regulate SAMHD1 activity and host restriction of human retroviral infection.

The demonstration that cytoplasmic RTI contributes to the elimination of HTLV-1-infected monocytes may have important consequences for human retroviral infection and pathogenesis. For example, the clearance of infected monocytes may prevent transmission to $CD4^+$ T cells, but would also deplete the precursor pool of myeloid dendritic cells that play a crucial role in controlling HTLV-1 infection (Rahman et al., 2011). Individuals suffering from ATL or HAM/TSP have been shown to possess a lower absolute number of DC than healthy individuals (Azakami et al., 2009; Hishizawa et al., 2004) and HTLV-1-infected monocytes also exhibit defective differentiation into DC (Makino et al., 2000; Nascimento et al., 2011). These factors may influence the development of HAM/TSP or ATL in HTLV-1 infected individuals, thus emphasizing the need to better understand the early host restriction of HTLV-1 infectivity by SAMHD1.

EXPERIMENTAL PROCEDURES

Products

RPMI-1640 media, FBS and antibiotics were provided by Wisent Technologies (CA, USA). All monoclonal antibodies (mAbs) and products used for flow cytometry were purchased from Biolegend (CA, USA), except for anti-cleaved caspase 3-PE mAbs, Annexin-V buffer 10X and Annexin-V-V450 obtained from Becton Dickinson (NJ, USA). Anti-p19 mAbs (clone TP-7) was purchased from ZeptoMetrix Corporation (NY, USA), whereas anti-gp46 mAbs (clone 67/5.5.13.1) was purchased from Abcam (MA, USA). Anti-Tax-FITC mAbs (clone LT4) was generously provided by Dr. Yuetsu Tanaka (Kitasato University, Kanagawa, Japan). All antibodies included in western blotting analyses came from Cell signaling Biotechnology Inc. (MA, USA), except for anti-Bax mAbs (Santa Cruz Biotechnology Inc.; TX, USA). Pan-caspase inhibitor Z-VAD-FMK (ZVAD) was purchased from R & D Systems^{R} (MN, USA). All cell lines were obtained from the ATCC^{TM} (VA, USA).

Purification of monocytes

Leukaphereses from healthy donors were obtained from the Royal Victoria Hospital, Montreal (QC, Canada), with informed consent of the patients and in agreement with the Royal Victoria Hospital, the Jewish General Hospital, and McGill University Research Ethics Committee.

HTLV-1 purification and *in vitro* infection

HTLV-1 viruses were purified from MT-2 supernatants. Cells were seeded overnight in complete RPMI (2.10^6 cells/mL). Supernatants were collected and ultra-centrifuged for 2h at 30,000 g at 4ºC. The viral pellet was re-suspended in complete RPMI, and HTLV-1 particles were quantified by gag p19 ELISA assays (ZeptoMetrix). 200,000 purified monocytes were incubated with 2µg HTLV-1 for 3h at 37ºC in 0.5 mL RPMI complete with or without 100µM Z-VAD-FMK. To

specifically block HTLV-1 infection, neutralizing anti-gp46 mAbs (at 10µg/mL; Abcam) were incubated 30 minutes at 4ºC with HTLV-1 prior *in vitro* infection. At 3h pi, monocytes were washed twice in complete RPMI and then co-cultured with 8.10^5 autologous monocyte-depleted PBMCs (1 ml complete RPMI; [HTLV-1] = 2µg/mL).

Western blotting

Protein lysates (2-10 µg) from monocytes were subjected to Western blot analysis as previously described (Oliere et al., 2010).

Small interfering RNA assays

10^7 purified monocytes were electroporated in the presence of control or specific siRNA using Nucleofactor II technology according the manufacturer's protocol (Amaxa human monocyte nucleofactor kit).

Biotinylated retroviral DNA_{90} assay

Retroviral DNA was produced by Integrated DNA technologies (IA, USA). HTLV-1 $ssDNA_{90}$ is the reverse complement of the 5'utr region (315-404 of complete HTLV-1 genome; NCBI) that is 90 bases long and conjugated with biotin on the 5' end. 10^7 monocytes were transfected with 10µg $vDNA_{90}$ for 24h in RPMI + 30% FBS in the absence of antibiotics. Monocytes were washed and then co-cultured in complete RPMI with $CD14^{neg}$PBMCs.

STING pull-down and Bax co-immunoprecipitation

Monocytes were infected with HTLV1 or transfected with biotinylated RTI for 6h (pull-down) or 3h (co-IP). Monocytes were lysed using CHAPS buffer with protease inhibitors as previously described (Samuel et al., 2010). 3µg protein was collected and referred to as the "input" fraction.

Statistical analysis

Statistical analyses were performed using the non-parametric Mann-Whitney *U* test, assuming independent samples. However, differences among the treatment groups performed with n = 3 samples were analyzed by the parametric unpaired Student *t* test. *P* values of less than 0.05 were considered statistically significant. ***, $P < 0.001$; **, $P < 0.01$ and *, $P < 0.05$.

REFERENCES

Abe, T., Harashima, A., Xia, T., Konno, H., Konno, K., Morales, A., Ahn, J., Gutman, D., and Barber, G.N. (2013). STING Recognition of Cytoplasmic DNA Instigates Cellular Defense. Mol Cell *50*, 5-15.

Ayinde, D., Casartelli, N., and Schwartz, O. (2012). Restricting HIV the SAMHD1 way: through nucleotide starvation. Nat Rev Microbiol *10*, 675-680.

Azakami, K., Sato, T., Araya, N., Utsunomiya, A., Kubota, R., Suzuki, K., Hasegawa, D., Izumi, T., Fujita, H., Aratani, S., *et al.* (2009). Severe loss of invariant NKT cells exhibiting anti-HTLV-1 activity in patients with HTLV-1-associated disorders. Blood *114*, 3208-3215.

Baldauf, H.M., Pan, X., Erikson, E., Schmidt, S., Daddacha, W., Burggraf, M., Schenkova, K., Ambiel, I., Wabnitz, G., Gramberg, T., *et al.* (2012). SAMHD1 restricts HIV-1 infection in resting CD4(+) T cells. Nat Med *18*, 1682-1687.

Barber, G.N. (2011). Innate immune DNA sensing pathways: STING, AIMII and the regulation of interferon production and inflammatory responses. Curr Opin Immunol *23*, 10-20.

Berger, A., Sommer, A.F., Zwarg, J., Hamdorf, M., Welzel, K., Esly, N., Panitz, S., Reuter, A., Ramos, I., Jatiani, A., *et al.* (2011). SAMHD1-deficient CD14+ cells from individuals with Aicardi-Goutieres syndrome are highly susceptible to HIV-1 infection. PLoS Pathog *7*, e1002425.

Blasius, A.L., and Beutler, B. (2010). Intracellular toll-like receptors. Immunity *32*, 305-315.

Burdette, D.L., and Vance, R.E. (2013). STING and the innate immune response to nucleic acids in the cytosol. Nat Immunol *14*, 19-26.

Chattopadhyay, S., Fensterl, V., Zhang, Y., Veleeparambil, M., Yamashita, M., and Sen, G.C. (2013). Role of interferon regulatory factor 3-mediated apoptosis in the establishment and maintenance of persistent infection by Sendai virus. J Virol *87*, 16-24.

Chattopadhyay, S., Marques, J.T., Yamashita, M., Peters, K.L., Smith, K., Desai, A., Williams, B.R., and Sen, G.C. (2010). Viral apoptosis is induced by IRF-3-mediated activation of Bax. EMBO J *29*, 1762-1773.

Chattopadhyay, S., Yamashita, M., Zhang, Y., and Sen, G.C. (2011). The IRF-3/Bax-mediated apoptotic pathway, activated by viral cytoplasmic RNA and DNA, inhibits virus replication. J Virol *85*, 3708-3716.

Colisson, R., Barblu, L., Gras, C., Raynaud, F., Hadj-Slimane, R., Pique, C., Hermine, O., Lepelletier, Y., and Herbeuval, J.P. (2010). Free HTLV-1 induces TLR7-dependent innate immune response and TRAIL relocalization in killer plasmacytoid dendritic cells. Blood *115*, 2177-2185.

Cook, L.B., Elemans, M., Rowan, A.G., and Asquith, B. (2013). HTLV-1: persistence and pathogenesis. Virology *435*, 131-140.

Cribier, A., Descours, B., Valadao, A.L., Laguette, N., and Benkirane, M. (2013). Phosphorylation of SAMHD1 by Cyclin A2/CDK1 Regulates Its Restriction Activity toward HIV-1. Cell Rep.

Descours, B., Cribier, A., Chable-Bessia, C., Ayinde, D., Rice, G., Crow, Y., Yatim, A., Schwartz, O., Laguette, N., and Benkirane, M. (2012). SAMHD1 restricts HIV-1 reverse transcription in quiescent CD4(+) T-cells. Retrovirology *9*, 87.

Doitsh, G., Cavrois, M., Lassen, K.G., Zepeda, O., Yang, Z., Santiago, M.L., Hebbeler, A.M., and Greene, W.C. (2010). Abortive HIV infection mediates CD4 T cell depletion and inflammation in human lymphoid tissue. Cell *143*, 789-801.

Goldstone, D.C., Ennis-Adeniran, V., Hedden, J.J., Groom, H.C., Rice, G.I., Christodoulou, E., Walker, P.A., Kelly, G., Haire, L.F., Yap, M.W., *et al.* (2011). HIV-1 restriction factor SAMHD1 is a deoxynucleoside triphosphate triphosphohydrolase. Nature *480*, 379-382.

Goubau, D., Romieu-Mourez, R., Solis, M., Hernandez, E., Mesplede, T., Lin, R., Leaman, D., and Hiscott, J. (2009). Transcriptional re-programming of primary macrophages reveals distinct apoptotic and anti-tumoral functions of IRF-3 and IRF-7. Eur J Immunol *39*, 527-540.

Gramberg, T., Kahle, T., Bloch, N., Wittmann, S., Mullers, E., Daddacha, W., Hofmann, H., Kim, B., Lindemann, D., and Landau, N.R. (2013). Restriction of diverse retroviruses by SAMHD1. Retrovirology *10*, 26.

Hishizawa, M., Imada, K., Kitawaki, T., Ueda, M., Kadowaki, N., and Uchiyama, T. (2004). Depletion and impaired interferon-alpha-producing capacity of blood plasmacytoid dendritic cells in human T-cell leukaemia virus type I-infected individuals. Br J Haematol *125*, 568-575.

Hollenbaugh, J.A., Gee, P., Baker, J., Daly, M.B., Amie, S.M., Tate, J., Kasai, N., Kanemura, Y., Kim, D.H., Ward, B.M., *et al.* (2013). Host Factor SAMHD1 Restricts DNA Viruses in Non-Dividing Myeloid Cells. PLoS Pathog *9*, e1003481.

Igakura, T., Stinchcombe, J.C., Goon, P.K., Taylor, G.P., Weber, J.N., Griffiths, G.M., Tanaka, Y., Osame, M., and Bangham, C.R. (2003). Spread of HTLV-I between lymphocytes by virus-induced polarization of the cytoskeleton. Science *299*, 1713-1716.

Ishikawa, H., and Barber, G.N. (2008). STING is an endoplasmic reticulum adaptor that facilitates innate immune signalling. Nature *455*, 674-678.

Ishikawa, H., Ma, Z., and Barber, G.N. (2009). STING regulates intracellular DNA-mediated, type I interferon-dependent innate immunity. Nature *461*, 788-792.

Jones, K.S., Petrow-Sadowski, C., Bertolette, D.C., Huang, Y., and Ruscetti, F.W. (2005). Heparan sulfate proteoglycans mediate attachment and entry of human T-cell leukemia virus type 1 virions into CD4+ T cells. J Virol *79*, 12692-12702.

Jones, K.S., Petrow-Sadowski, C., Huang, Y.K., Bertolette, D.C., and Ruscetti, F.W. (2008). Cell-free HTLV-1 infects dendritic cells leading to transmission and transformation of CD4(+) T cells. Nat Med *14*, 429-436.

Kaushik, R., Zhu, X., Stranska, R., Wu, Y., and Stevenson, M. (2009). A cellular restriction dictates the permissivity of nondividing monocytes/macrophages to lentivirus and gammaretrovirus infection. Cell Host Microbe *6*, 68-80.

Kawai, T., and Akira, S. (2011). Toll-like receptors and their crosstalk with other innate receptors in infection and immunity. Immunity *34*, 637-650.

Kim, B., Nguyen, L.A., Daddacha, W., and Hollenbaugh, J.A. (2012). Tight interplay among SAMHD1 protein level, cellular dNTP levels, and HIV-1 proviral DNA synthesis kinetics in human primary monocyte-derived macrophages. J Biol Chem *287*, 21570-21574.

Kondo, T., Kobayashi, J., Saitoh, T., Maruyama, K., Ishii, K.J., Barber, G.N., Komatsu, K., Akira, S., and Kawai, T. (2013). DNA damage sensor MRE11 recognizes cytosolic double-

stranded DNA and induces type I interferon by regulating STING trafficking. Proc Natl Acad Sci U S A *110*, 2969-2974.

Kumar, H., Kawai, T., and Akira, S. (2011). Pathogen recognition by the innate immune system. Int Rev Immunol *30*, 16-34.

Laguette, N., and Benkirane, M. (2012). How SAMHD1 changes our view of viral restriction. Trends Immunol *33*, 26-33.

Laguette, N., Rahm, N., Sobhian, B., Chable-Bessia, C., Munch, J., Snoeck, J., Sauter, D., Switzer, W.M., Heneine, W., Kirchhoff, F., *et al.* (2012). Evolutionary and functional analyses of the interaction between the myeloid restriction factor SAMHD1 and the lentiviral Vpx protein. Cell Host Microbe *11*, 205-217.

Laguette, N., Sobhian, B., Casartelli, N., Ringeard, M., Chable-Bessia, C., Segeral, E., Yatim, A., Emiliani, S., Schwartz, O., and Benkirane, M. (2011). SAMHD1 is the dendritic- and myeloid-cell-specific HIV-1 restriction factor counteracted by Vpx. Nature *474*, 654-657.

Lahouassa, H., Daddacha, W., Hofmann, H., Ayinde, D., Logue, E.C., Dragin, L., Bloch, N., Maudet, C., Bertrand, M., Gramberg, T., *et al.* (2012). SAMHD1 restricts the replication of human immunodeficiency virus type 1 by depleting the intracellular pool of deoxynucleoside triphosphates. Nat Immunol *13*, 223-228.

Makino, M., Wakamatsu, S., Shimokubo, S., Arima, N., and Baba, M. (2000). Production of functionally deficient dendritic cells from HTLV-I-infected monocytes: implications for the dendritic cell defect in adult T cell leukemia. Virology *274*, 140-148.

Nascimento, C.R., Lima, M.A., de Andrada Serpa, M.J., Espindola, O., Leite, A.C., and Echevarria-Lima, J. (2011). Monocytes from HTLV-1-infected patients are unable to fully mature into dendritic cells. Blood *117*, 489-499.

Nisole, S., and Saib, A. (2004). Early steps of retrovirus replicative cycle. Retrovirology *1*, 9.

Oliere, S., Hernandez, E., Lezin, A., Arguello, M., Douville, R., Nguyen, T.L., Olindo, S., Panelatti, G., Kazanji, M., Wilkinson, P., *et al.* (2010). HTLV-1 evades type I interferon antiviral signaling by inducing the suppressor of cytokine signaling 1 (SOCS1). PLoS Pathog *6*, e1001177.

Pais-Correia, A.M., Sachse, M., Guadagnini, S., Robbiati, V., Lasserre, R., Gessain, A., Gout, O., Alcover, A., and Thoulouze, M.I. (2010). Biofilm-like extracellular viral assemblies mediate HTLV-1 cell-to-cell transmission at virological synapses. Nat Med *16*, 83-89.

Ragin, C., Edwards, R., Heron, D.E., Kuo, J., Wentzel, E., Gollin, S.M., and Taioli, E. (2008). Prevalence of cancer-associated viral infections in healthy afro-Caribbean populations: a review of the literature. Cancer Invest *26*, 936-947.

Rahman, S., Khan, Z.K., Wigdahl, B., Jennings, S.R., Tangy, F., and Jain, P. (2011). Murine FLT3 ligand-derived dendritic cell-mediated early immune responses are critical to controlling cell-free human T cell leukemia virus type 1 infection. J Immunol *186*, 390-402.

Rice, G.I., Bond, J., Asipu, A., Brunette, R.L., Manfield, I.W., Carr, I.M., Fuller, J.C., Jackson, R.M., Lamb, T., Briggs, T.A., *et al.* (2009). Mutations involved in Aicardi-Goutieres syndrome implicate SAMHD1 as regulator of the innate immune response. Nat Genet *41*, 829-832.

Samuel, S., Tumilasci, V.F., Oliere, S., Nguyen, T.L., Shamy, A., Bell, J., and Hiscott, J. (2010). VSV oncolysis in combination with the BCL-2 inhibitor obatoclax overcomes apoptosis resistance in chronic lymphocytic leukemia. Mol Ther *18*, 2094-2103.

Sun, L., Wu, J., Du, F., Chen, X., and Chen, Z.J. (2013). Cyclic GMP-AMP synthase is a cytosolic DNA sensor that activates the type I interferon pathway. Science *339*, 786-791.

Triques, K., and Stevenson, M. (2004). Characterization of restrictions to human immunodeficiency virus type 1 infection of monocytes. J Virol *78*, 5523-5527.

Unterholzner, L., Keating, S.E., Baran, M., Horan, K.A., Jensen, S.B., Sharma, S., Sirois, C.M., Jin, T., Latz, E., Xiao, T.S., *et al.* (2010). IFI16 is an innate immune sensor for intracellular DNA. Nat Immunol *11*, 997-1004.

Van Prooyen, N., Gold, H., Andresen, V., Schwartz, O., Jones, K., Ruscetti, F., Lockett, S., Gudla, P., Venzon, D., and Franchini, G. (2010). Human T-cell leukemia virus type 1 p8 protein increases cellular conduits and virus transmission. Proc Natl Acad Sci U S A *107*, 20738-20743.

Verdonck, K., Gonzalez, E., Van Dooren, S., Vandamme, A.M., Vanham, G., and Gotuzzo, E. (2007). Human T-lymphotropic virus 1: recent knowledge about an ancient infection. Lancet Infect Dis *7*, 266-281.

Welbourn, S., Miyagi, E., White, T.E., Diaz-Griffero, F., and Strebel, K. (2012). Identification and characterization of naturally occurring splice variants of SAMHD1. Retrovirology *9*, 86.

White, T.E., Brandariz-Nunez, A., Valle-Casuso, J.C., Amie, S., Nguyen, L.A., Kim, B., Tuzova, M., and Diaz-Griffero, F. (2013). The retroviral restriction ability of SAMHD1, but not its deoxynucleotide triphosphohydrolase activity, is regulated by phosphorylation. Cell Host Microbe *13*, 441-451.

Yamano, Y., and Sato, T. (2012). Clinical pathophysiology of human T-lymphotropic virus-type 1-associated myelopathy/tropical spastic paraparesis. Front Microbiol *3*, 389.

Yan, N., Regalado-Magdos, A.D., Stiggelbout, B., Lee-Kirsch, M.A., and Lieberman, J. (2010). The cytosolic exonuclease TREX1 inhibits the innate immune response to human immunodeficiency virus type 1. Nat Immunol *11*, 1005-1013.

Zhang, Z., Yuan, B., Bao, M., Lu, N., Kim, T., and Liu, Y.J. (2011). The helicase DDX41 senses intracellular DNA mediated by the adaptor STING in dendritic cells. Nat Immunol *12*, 959-965.

Zhong, B., Yang, Y., Li, S., Wang, Y.Y., Li, Y., Diao, F., Lei, C., He, X., Zhang, L., Tien, P., *et al.* (2008). The adaptor protein MITA links virus-sensing receptors to IRF3 transcription factor activation. Immunity *29*, 538-550.

ACKNOWLEDGMENTS

We are grateful to the donors who participated in this study, as well as Dr. JP Routy, Royal Victoria Hospital and the attending staff. This project was supported by research funds from VGTI Florida and the Canadian Institutes of Health Research (#MOP-106686).

AUTHOR CONTRIBUTIONS

AS performed most of the experiments and helped write the paper; SMB and RL aided in the STING pull-down and anti-Bax co-immunoprecipitation experiments; DO helped to write the paper and edited text and Figures; JH and JvG conceived the study, designed experiments, supervised the experiments, and wrote the paper.

COMPETITING FINANCIAL INTERESTS

The authors declare no competing financial interests.

FIGURE LEGENDS

Figure 1. Early type I IFN response in monocytes following abortive HTLV-1 infection. (A-C) Purified monocytes were infected with HTLV-1 for 3h and then co-cultured with the autologous $CD14^{neg}$PBMCs for 120h pi. (A) Virus binding to isolated monocytes at 3h pi in response to various HTLV-1 concentrations, as analyzed by flow cytometry with anti-gp46 Abs. *P* values were determined based on the comparison with cells infected with 5µg/mL HTLV-1 (n = 5). (B) At 3-120h pi, total RNA was extracted from monocytes and analyzed for HTLV-1 viral load using primers located in the 5' untranslated region (5'utr) of HTLV-1 genome (Table S1). Equivalent vRNA amounts were normalized to β-actin mRNA expression and calculated as fold change from the level of uninfected monocytes (arbitrary set as 1). Jurkat and MT-2 cells were used as negative and positive control respectively (n = 5). (C) At 3, 24 and 48h pi, levels of HTLV-1 binding, viral internalization and *de novo* production of viral proteins were assessed on monocytes by gp46 surface staining, p19 and Tax ICS, respectively. Histograms are representative of raw data from 5 independent experiments. The mean relative expression ± SD for all conditions are also indicated in bold. MT-2 and Jurkat cell lines were used as positive and negative controls for all stainings, respectively. (D) p24 expression and type I IFN responses were investigated by immunoblotting on purified monocytes (n = 3).

Figure 2. HTLV-1-infected monocytes undergo mitochondrial-dependent apoptosis. (A) The percentage of apoptosis on gated $CD3^{-}CD14^{+}$monocytes was assessed by Annexin-V staining at 3-120h pi. *P* values were determined by the comparison with uninfected cells (n = 5). (B) Levels of Annexin-V, $_{CL}$caspase-3 and p19 expression determined at 48h pi on monocytes, treated or not with ZVAD or with α-gp46 mAb. Representative histograms from five independent experiments are shown above. (C) At 48h pi, the loss of mitochondrial membrane

potential on monocytes in the presence or absence of ZVAD or α-gp46 mAb was evaluated by flow cytometry using the fluorescent dye $DiOC_6(3)$. Results shown represent the percentage of $CD3^-CD14^+DiOC_6(3)^{low}$ monocytes, as indicated above in the representative histograms (n = 5). (D) The correlations between the percentage of apoptotic monocytes and (*i*) $_{CL}$caspase-3 expression, or (*ii*) mitochondrial depolarisation were calculated in infected monocytes during the course of the co-culture (n = 25; Spearman test). (E) Expression levels of p24, Bcl-2 family members and caspase 9 cleavage were assessed by immunoblotting at 3h pi (n = 3).

Figure 3. SAMHD1 drives apoptosis in HTLV-1-infected monocytes. (A-C) Monocytes were transfected with control or SAMHD1 siRNA for 3d, and then subsequently infected with HTLV-1 for 48h. (A) Efficiency of SAMHD1 silencing was determined at day 3 by immunoblotting. (n = 5). No changes were observed in the levels of total ERK_2 expression, confirming the specificity of SAMHD1 silencing. (B) Levels of apoptosis and intracellular p19 on transfected $CD14^+$monocytes at 48h pi. Results represent the HTLV-1-induced apoptosis determined on transfected monocytes using the formula: % of apoptosis in infected cells - % of apoptosis in uninfected cells. Data are expressed as mean ± SD for five independent experiments, including the inhibition of apoptosis (%) when SAMHD1 was silenced (indicated in blue). The flow histograms shown on the right side are representative of raw data. (C) Correlation between the inhibition of SAMHD1 expression and HTLV-1-induced apoptosis determined on transfected monocytes (n = 5 [values from Figs. 3A, B]; Spearman test). (D) Levels of apoptosis determined on monocytes in the presence of increasing doses of exogenous dN at 48h pi. Percentage of apoptosis inhibition determined on infected cells in the presence of dN are also indicated in blue. Statistical analyses are based on the comparison to untouched monocytes, except for those

indicated in bold, that are calculated when compared to HTLV-1-infected, non-dN-treated monocytes (n = 5).

Figure 4. **Cytosolic RTI induces monocyte apoptosis following HTLV-1 infection**. (A) At 24h pi, DNA was extracted from total (TF) and nuclear (NF) fractions in monocytes. Viral load was determined by qPCR using 5´utr primers and normalized to erv-3. Results shown represent the relative fold change and statistical analyses, compared to uninfected monocytes (n = 5). Purity of NF was determined by immunoblotting using antibodies against nuclear (Thoc-1 and $Histone_{H3}$) and cytosolic (COX-IV) proteins. (B) Monocytes were transfected with SAMHD1 siRNA, treated with exogenous 100nM dN, then treated as in (A). Results represent relative fold change compared to uninfected cells treated with control siRNA (n = 5). (C) Fold change of vDNA determined in monocytes at 48h pi using several pairs of primers and relative to infected monocytes without AZT. (D) Levels of apoptosis on monocytes in the presence or absence of AZT at 48h pi. Inhibition of apoptosis mediated by AZT is indicated in blue. (E) Fold change of vDNA performed in monocytes expressing or not SAMHD1 at 24h pi using several primer pairs. (F) The addition of HTLV-1 RTI in monocytes initiates apoptosis. Purified monocytes were transfected with scrambled, with HTLV-1 ss or $dsDNA_{90}$. At 48h post-transfection, cells were labeled with Annexin-V-V450, CD14-APC H7, and streptavidin-APC. Streptavidin-APC ICS allowed the distinction between monocytes that were $vDNA^{neg}$ (purple) or $vDNA^{+}$cells (green) in the same sample. Elect. = electroporated only; scram. = scrambled $ssDNA_{90}$. Values represent the percentages of normalized apoptosis indicated by the formula: % of apoptosis in RTI-transfected monocytes with siRNA - % of apoptosis in electroporated-only cells. Apoptosis mediated on primary monocytes by the electroporation methods averaged between ~15-19%. Flow histograms shown above are representative of raw data from five independent experiments.

Figure 5. STING complex formation with HTLV-1 DNA induces apoptosis in monocytes. (A) Monocytes were transfected with scrambled and HTLV-1 ss, or $dsDNA_{90}$ for 6h. As a negative control, 1 µg of HTLV-1 ssDNA was incubated with 1µl DNAse (Ambion; TX, USA) for 1h at 37ºC. STING and RIG-I pull-down was performed from monocyte lysates via interactions with biotinylated DNA (*Methods* section). Input lysates were also analyzed by immunoblot for expression of several proteins including STING, Bax, β-actin and ISG (n = 3). (B-D) STING regulates the premature death of infected monocytes. Purified monocytes were transfected with STING siRNA for 3 days and (B) the efficiency of STING silencing was determined via immunoblotting. (C) Annexin-V staining determined on transfected $CD14^+$monocytes at 48h pi. Values represent the % HTLV-1 induced apoptosis as determined by the formula: % apoptosis in infected cells - % apoptosis in uninfected cells. Inhibition of HTLV-1-mediated apoptosis following STING silencing is indicated in blue. Flow histograms shown on the right side are representative of raw data from five independent experiments. (D) Correlation between inhibition of STING expression and HTLV-1-mediated apoptosis on transfected monocytes (n = 5; Spearman test).

Figure 6. STING activation leads to the formation of the IRF3-Bax complex. (A) Monocytes were transfected with STING siRNA and expression of viral and host proteins (p24, STING, Bax, ISG and p-IRF3) was determined by immunoblotting at 3 and 48h pi. Representative blots from three independent experiments are shown. (B, C) Anti-Bax co-immunoprecipitations (co-IP) were performed at 6h pi (B) following *in vitro* infection or transfection with HTLV-1 DNA, (C) or in the context of (*i*) SAMHD1 and (*ii*) STING silencing. Inputs were also analyzed for the expression of several proteins. * = cross-linked isotype IgG_1 antibody (iso. IgG) used during co-

IP as negative control; performed on monocytes transfected with $ssDNA_{90}$. (D) At 24h pi, a multi-parametric antibody cocktail with $DiOC_6(3)$ dye, Annexin-V-V450, anti-CD14-APC H7, and anti-Bax-APC antibodies was used on co-cultured monocytes (n = 5). Anti-Bax antibody was conjugated to Alexa647 dye using the Zenon^R mouse IgG_1 labeling kit. Isotype IgG_1 control was used to determine the positivity of Bax expression. Results shown represent flow cytometry gating strategy based on HTLV-1-infected monocytes transfected with control siRNA. Bax^{neg} (green) versus Bax^+monocytes (red) were analyzed for mitochondrial depolarization and apoptosis. Percentages of $DiOC_6(3)^{low}$Annexin-V^+cells were indicated for both subsets. (E) Monocytes were transfected with Bax siRNA for 3h prior to HTLV-1 infection. Levels of HTLV-1-induced apoptosis were then investigated at 48h pi. Results are expressed as mean ± SD for three independent experiments, included in blue is the inhibition of apoptosis during Bax silencing. Bax knockdown was confirmed by immunoblotting 48h pi.

Figure 7. STING recognition of HIV-1 RTI leads to IRF3-Bax interaction and mitochondrial-dependent apoptosis. (A) Expression of STING, IRF3, P-IRF3 and Bax proteins were assessed by immunoblotting on monocytes transfected with HIV-1 $ssDNA_{90}$ for 3h. (B) STING pull-down and (C) anti-Bax co-IP were performed on monocytes transfected with HIV-1 $ssDNA_{90}$ (n = 3). (D) Monocytes treated with HIV-1 $ssDNA_{90}$ displayed higher levels of mitochondria-dependent apoptosis. At 48h pi, levels of Annexin-V, mitochondria depolarization (% of $DiOC_6(3)^{low}$cells) and co-staining were assessed on gated $CD14^+$monocytes in the presence of HIV-1 RTI. Results show the percentages of HIV-1-induced apoptosis and Bax expression, determined by the formula: % of staining in HIV-1 RTI-transfected monocytes - % of staining in monocytes electroporated alone. Flow histograms shown on the right side are representative of raw data from five independent experiments.

Figure

Figure 1

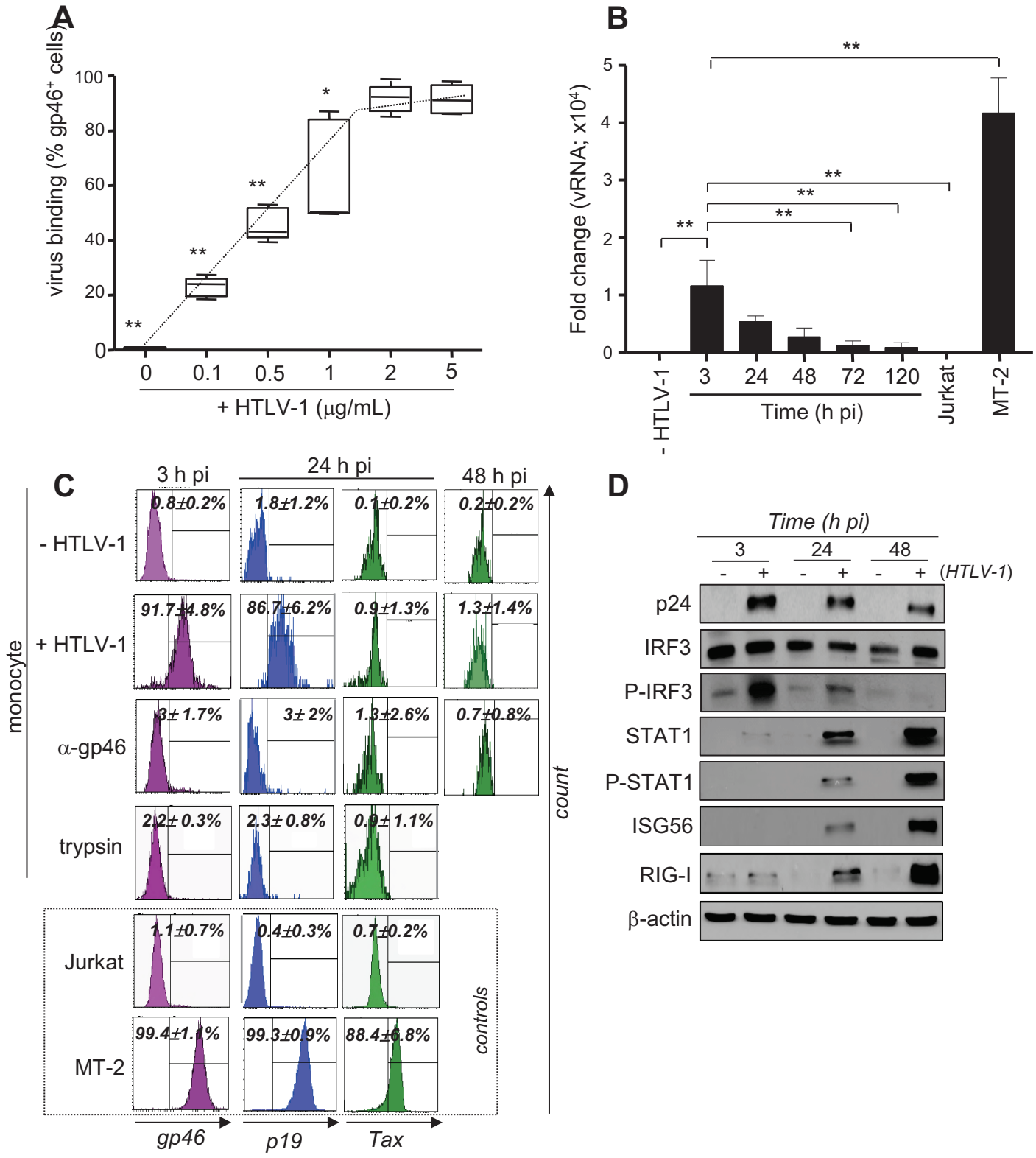

Figure

Figure 2

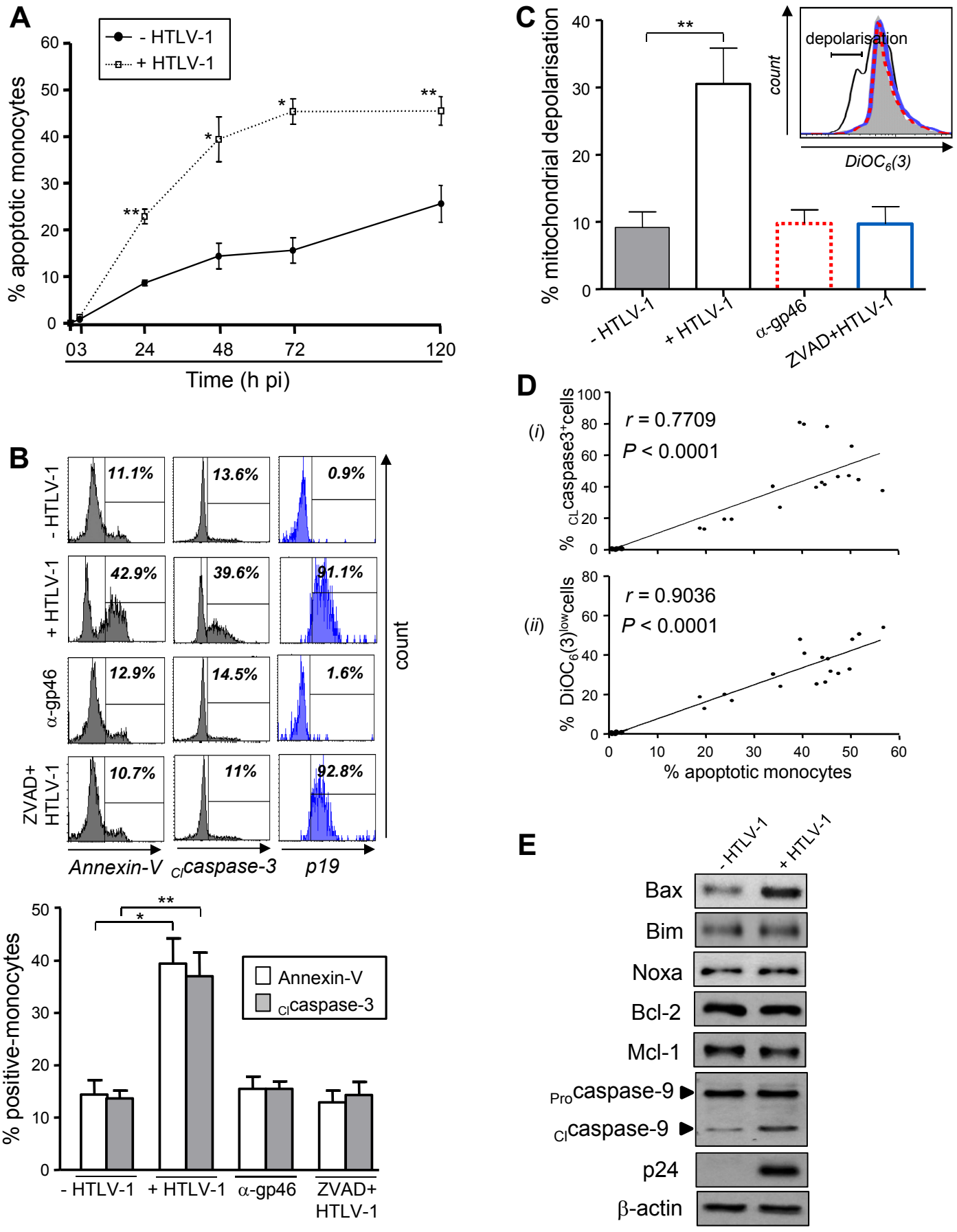

Figure

Figure 3

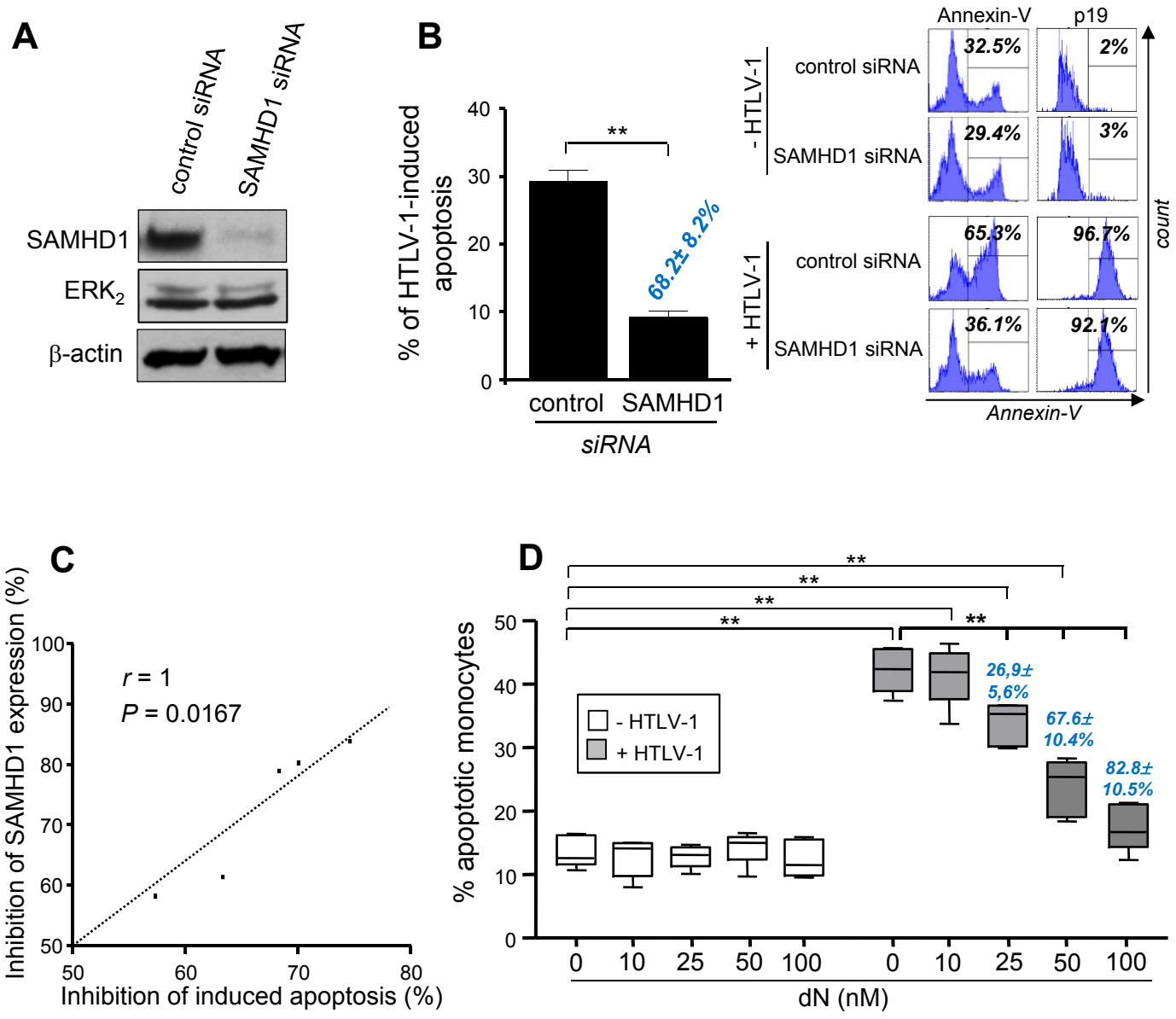

Figure

Figure 4

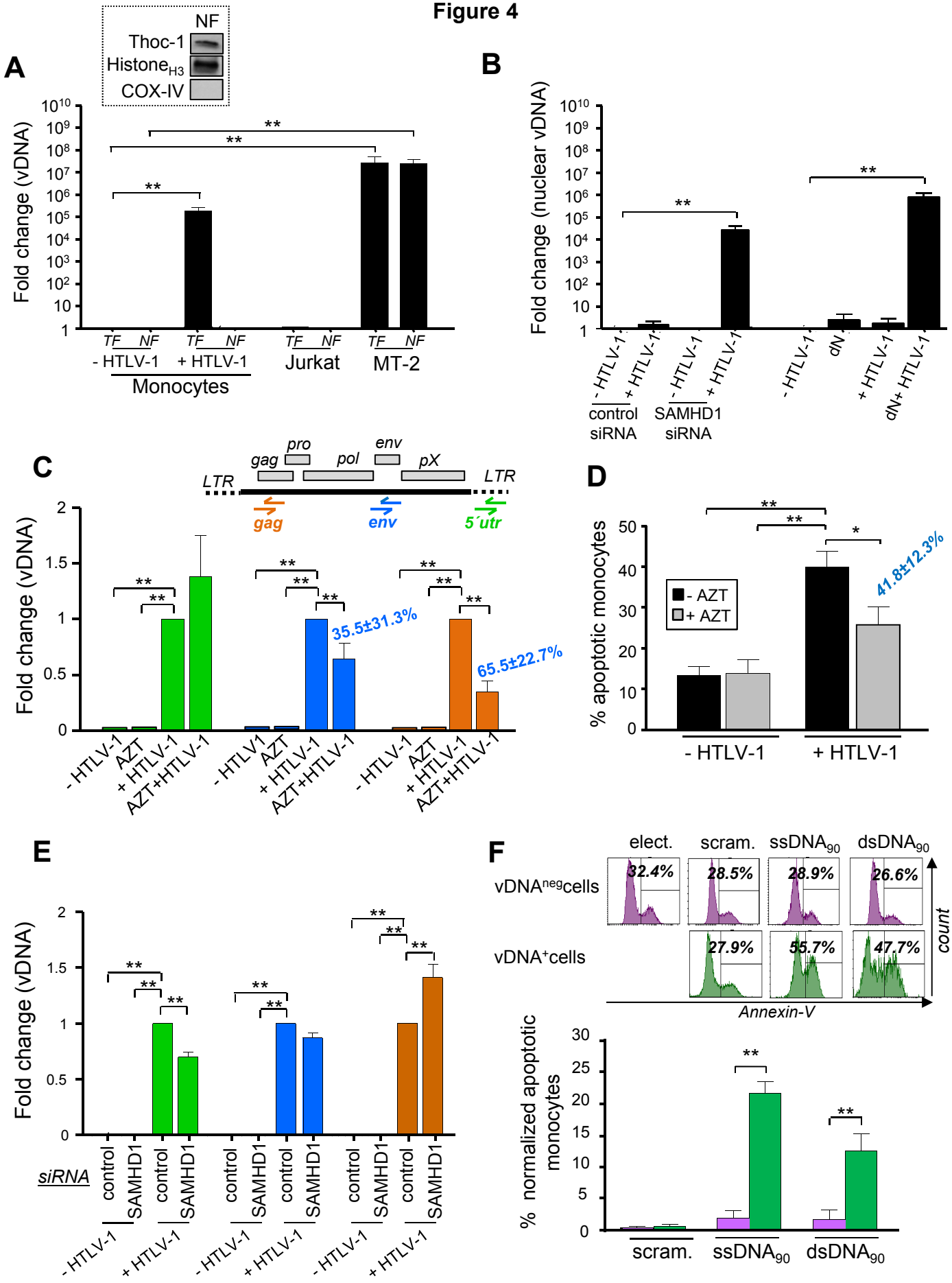

Figure

Figure 5

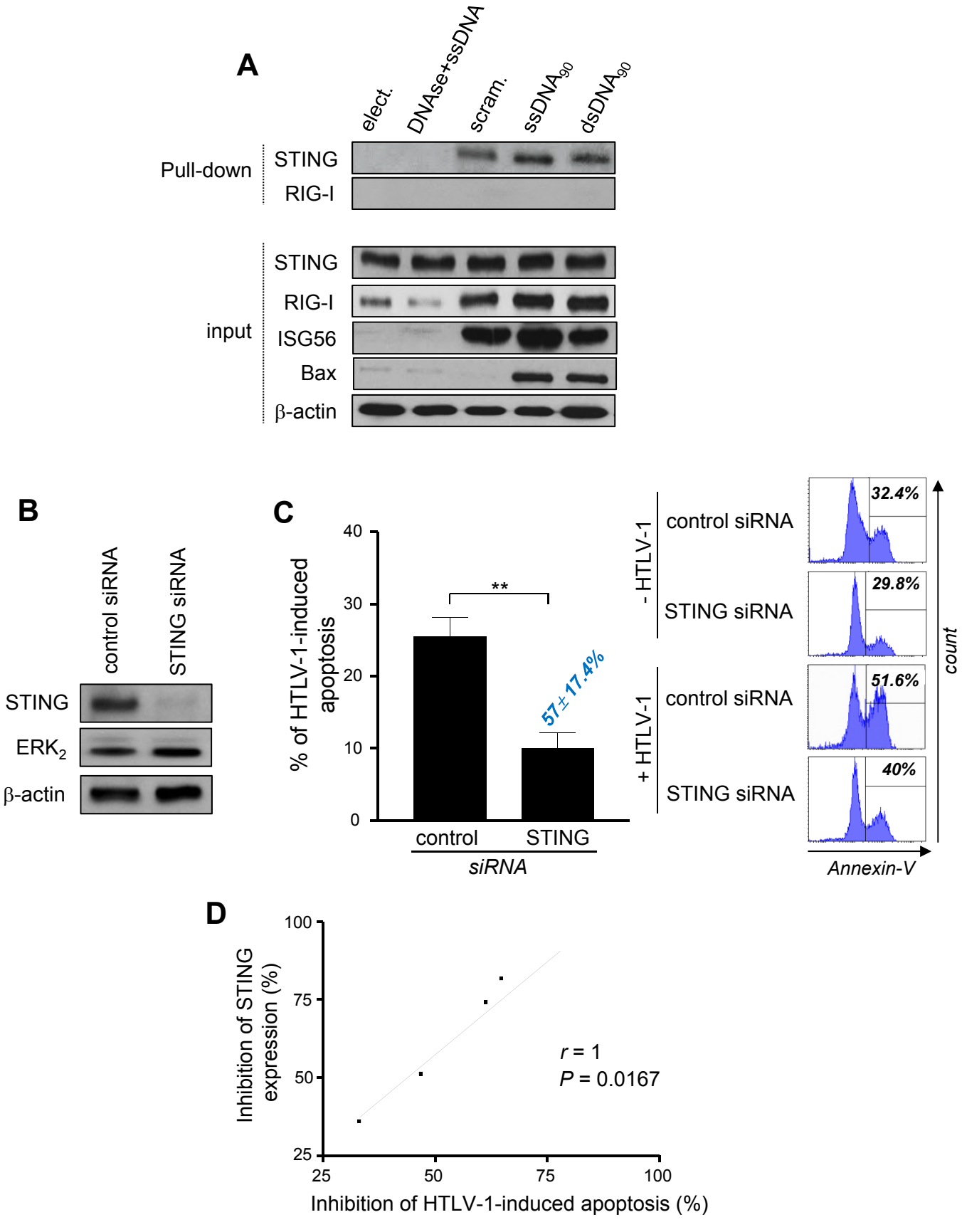

Figure

Figure 6

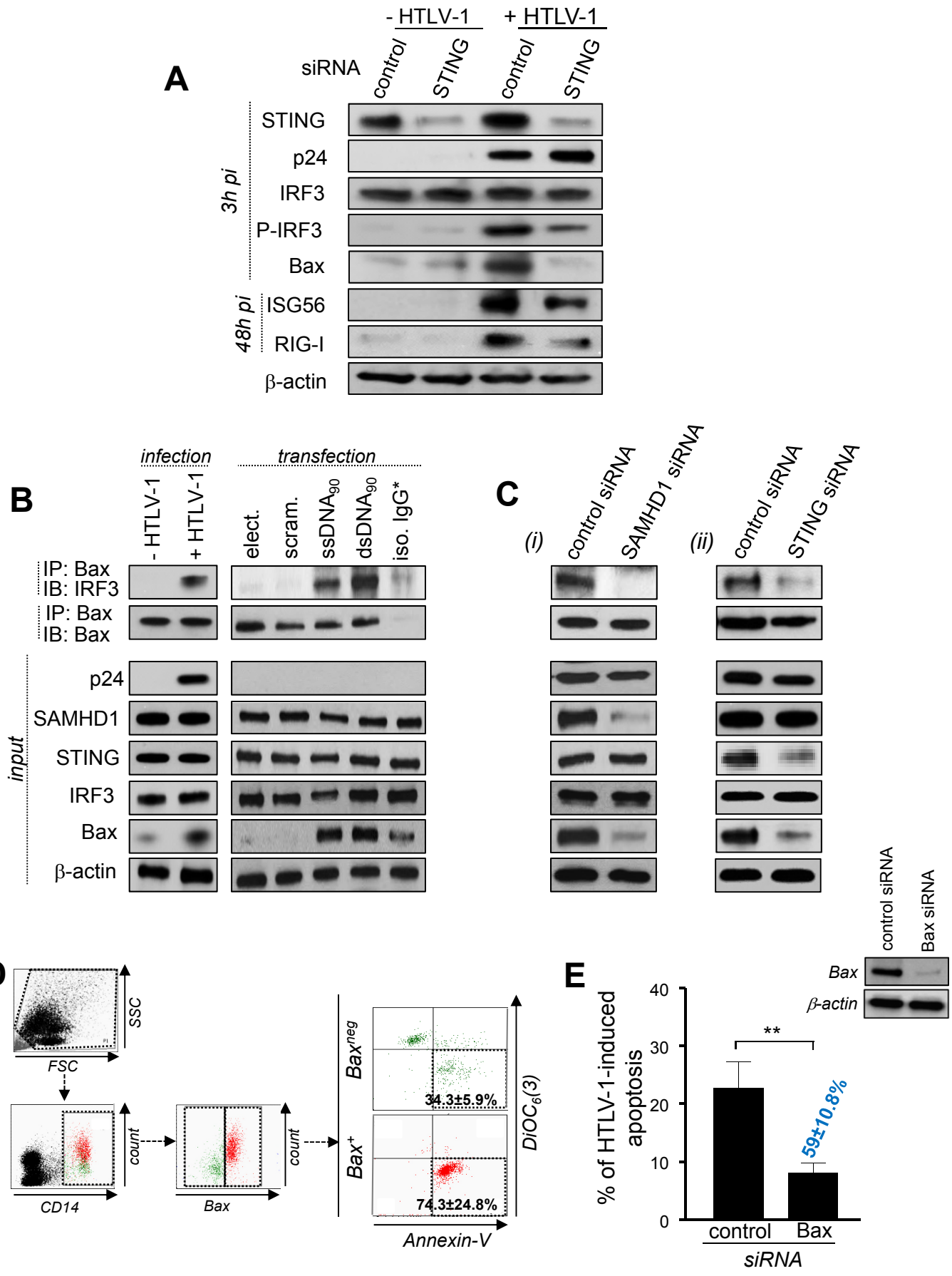

Figure

Figure 7

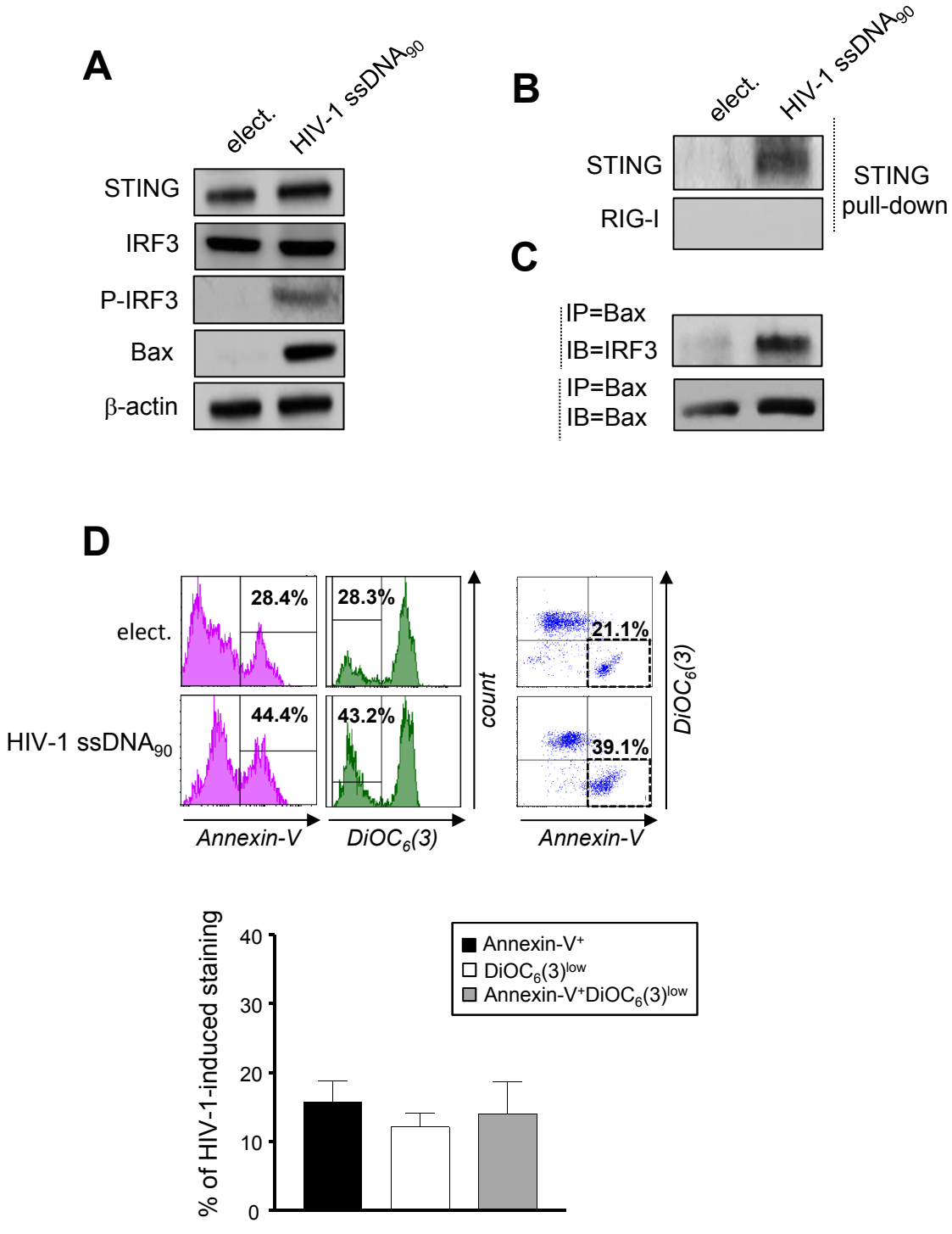

Inventory of Supplemental Information

Table S1

Housekeeping gene
HTLV-1 gene

localisation	*Orientation*	Sequence
β- actin	*forward*	ACTGGGACGACATGGAGAAAA
	reverse	GCCACACGCAGCTC
erv-3	*forward*	CATGGGAAGCAAGGGAACTAATG
	reverse	CCCAGCGAGCAATACAGAATTT
alu	*forward*	GCCTCCCAAAGTGCTGGGATTACAG
5´utr	*forward*	TTCGTTTTCTGTTCTGCGCC
	reverse	GCTATAGAATGGGCTGTCGCT
gag	*forward*	CCCTCCAGTTACGATTTCCA
	reverse	GGCTTGGGTTTGGATGAGTA
env	*forward*	CATCCCGGTAAGCGCTAGTT
	reverse	AAAGTGGCGAGAAACTTACCC

Figure S1

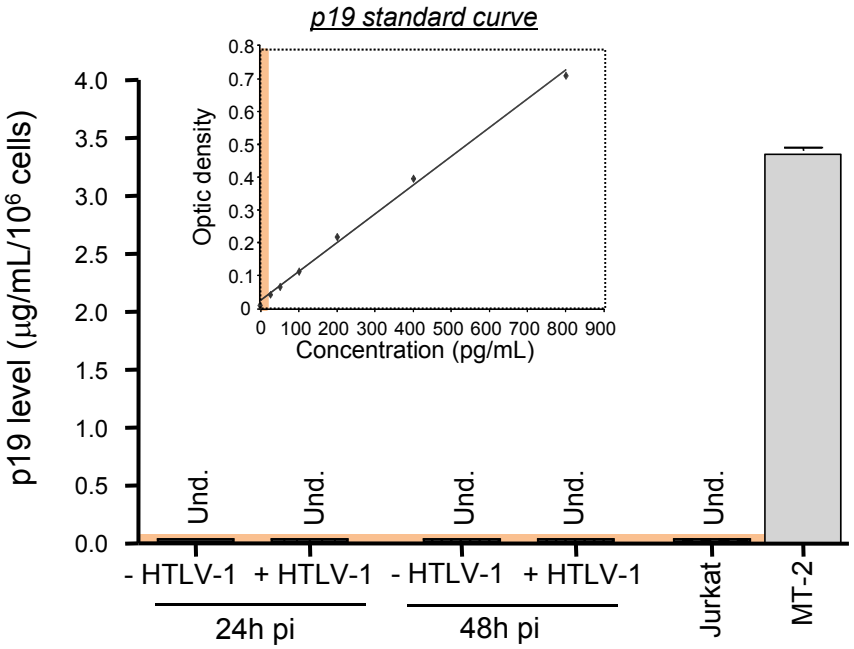
p19 standard curve
Optic density
Concentration (pg/mL)
p19 level (µg/mL/10^6 cells)
Und.
- HTLV-1
+ HTLV-1
24h pi
48h pi
Jurkat
MT-2

Figure S2

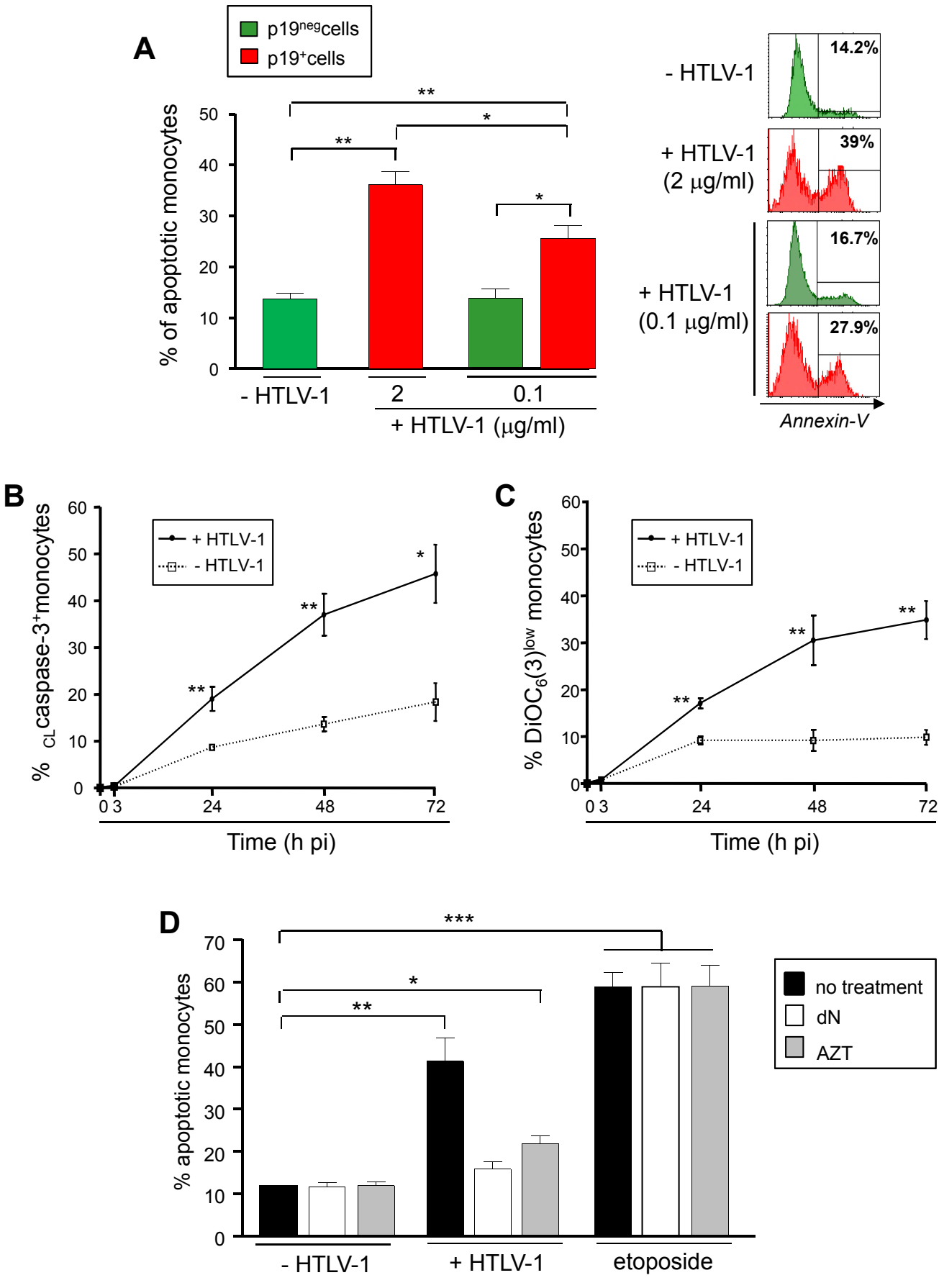
A
p19neg cells
p19+ cells
% of apoptotic monocytes
- HTLV-1
2
0.1
+ HTLV-1 (μg/ml)
14.2%
39%
16.7%
27.9%
Annexin-V
B
% CL caspase-3+ monocytes
+ HTLV-1
- HTLV-1
Time (h pi)
C
% DiOC6(3)low monocytes
+ HTLV-1
- HTLV-1
Time (h pi)
D
% apoptotic monocytes
no treatment
dN
AZT
- HTLV-1
+ HTLV-1
etoposide

Figure S3

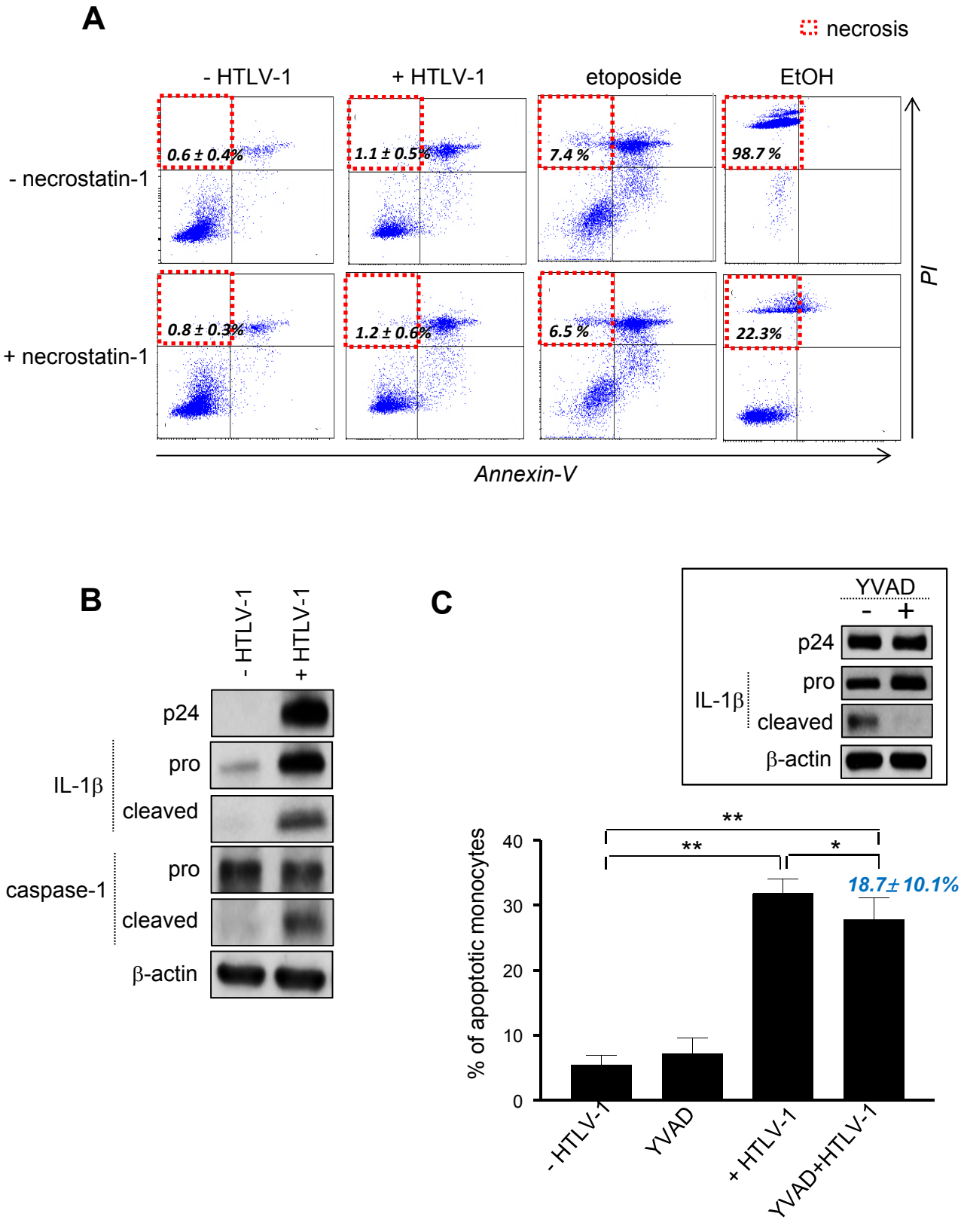
A
necrosis
- HTLV-1
+ HTLV-1
etoposide
EtOH
- necrostatin-1
+ necrostatin-1
0.6 ± 0.4%
1.1 ± 0.5%
7.4 %
98.7 %
0.8 ± 0.3%
1.2 ± 0.6%
6.5 %
22.3%
PI
Annexin-V
B
- HTLV-1
+ HTLV-1
p24
IL-1β
pro
cleaved
caspase-1
pro
cleaved
β-actin
C
YVAD
- +
p24
IL-1β
pro
cleaved
β-actin
% of apoptotic monocytes
0
10
20
30
40
**
**
*
18.7± 10.1%
- HTLV-1
YVAD
+ HTLV-1
YVAD+HTLV-1

Figure S4

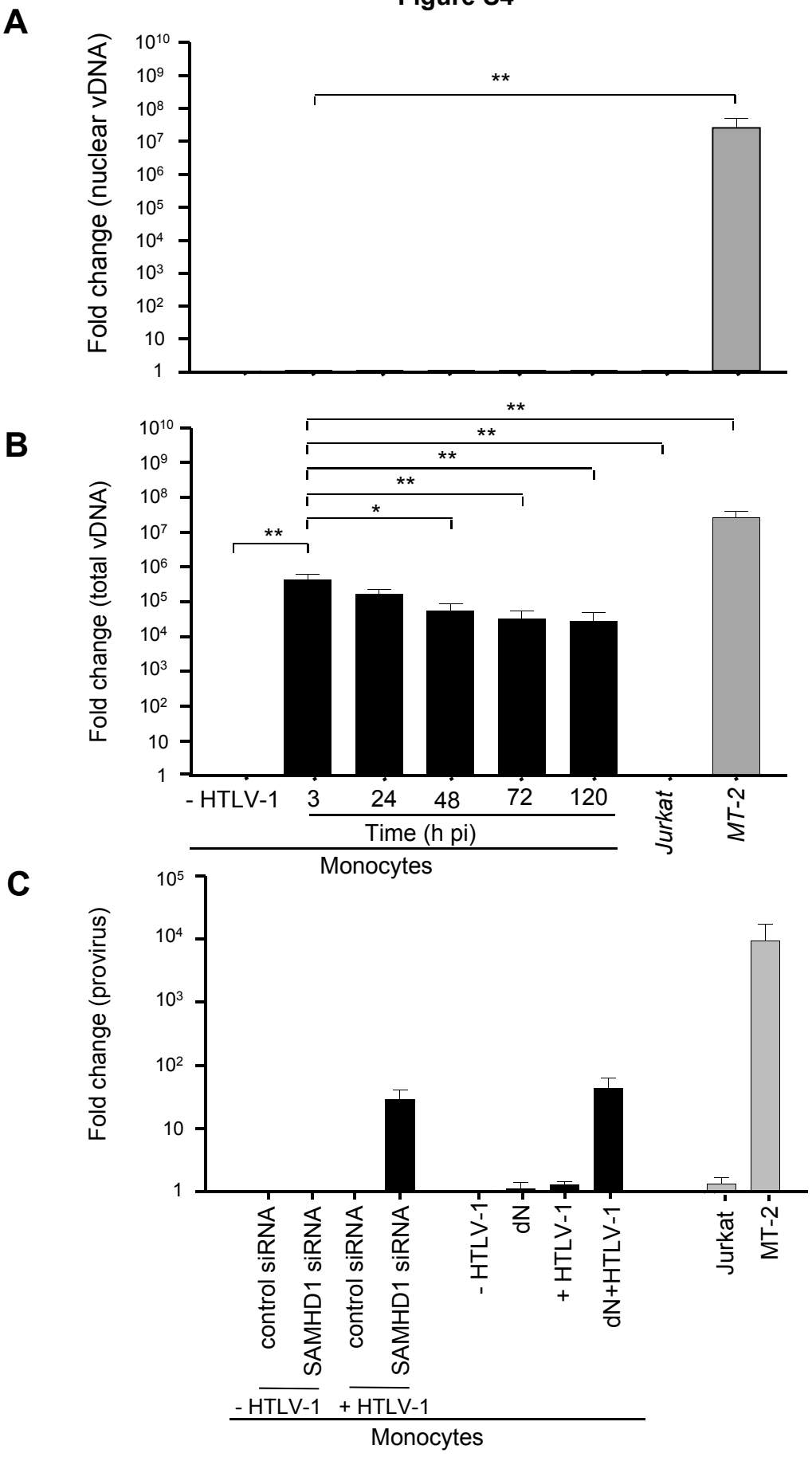
A
Fold change (nuclear vDNA)
B
Fold change (total vDNA)
- HTLV-1
3
24
48
72
120
Time (h pi)
Monocytes
Jurkat
MT-2
C
Fold change (provirus)
control siRNA
SAMHD1 siRNA
control siRNA
SAMHD1 siRNA
- HTLV-1
dN
+ HTLV-1
dN+HTLV-1
Jurkat
MT-2
- HTLV-1
+ HTLV-1
Monocytes

Figure S5

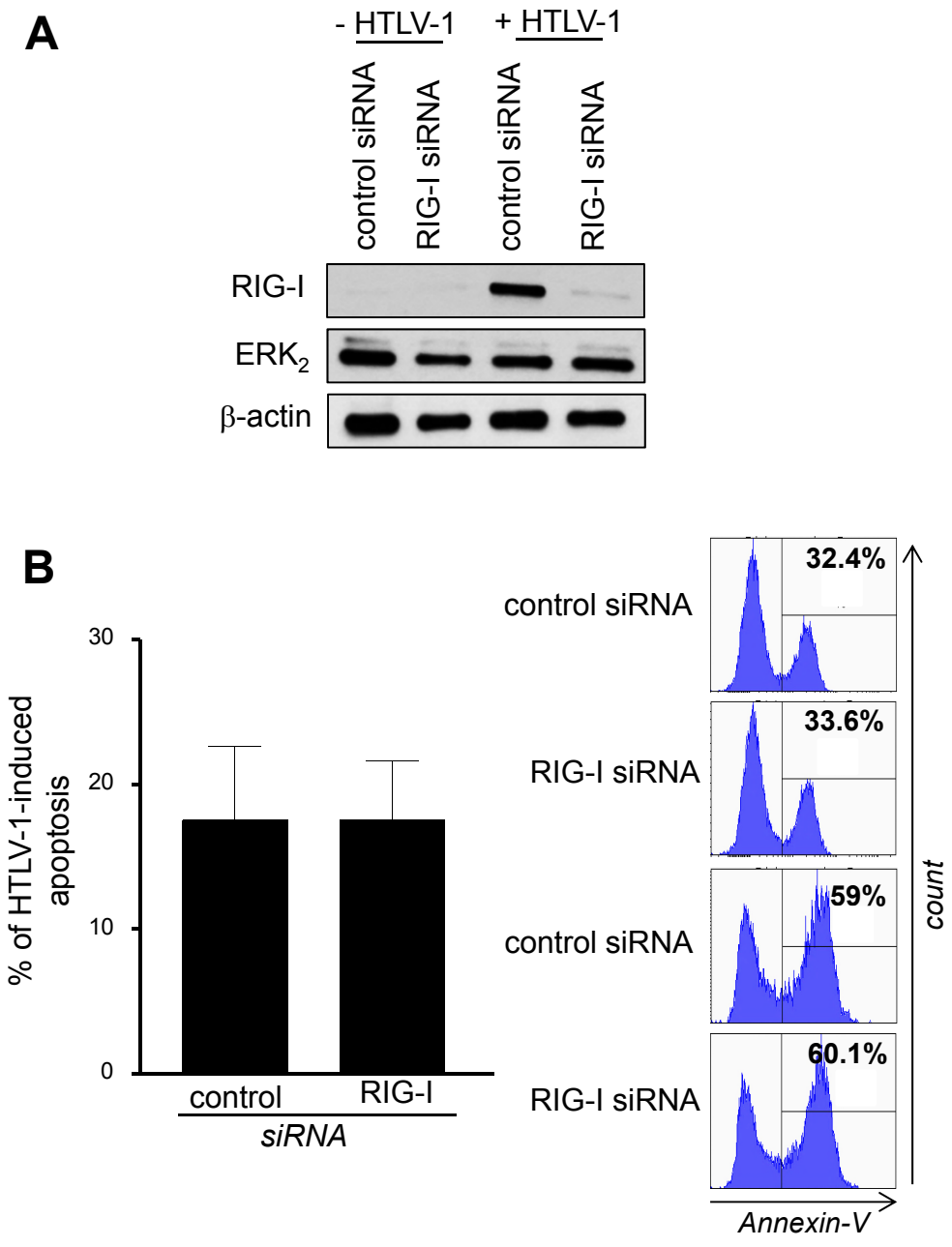
A
- HTLV-1
+ HTLV-1
control siRNA
RIG-I siRNA
control siRNA
RIG-I siRNA
RIG-I
ERK2
β-actin
B
% of HTLV-1-induced apoptosis
30
20
10
0
control
RIG-I
siRNA
control siRNA
32.4%
RIG-I siRNA
33.6%
control siRNA
59%
RIG-I siRNA
60.1%
count
Annexin-V

Figure S6

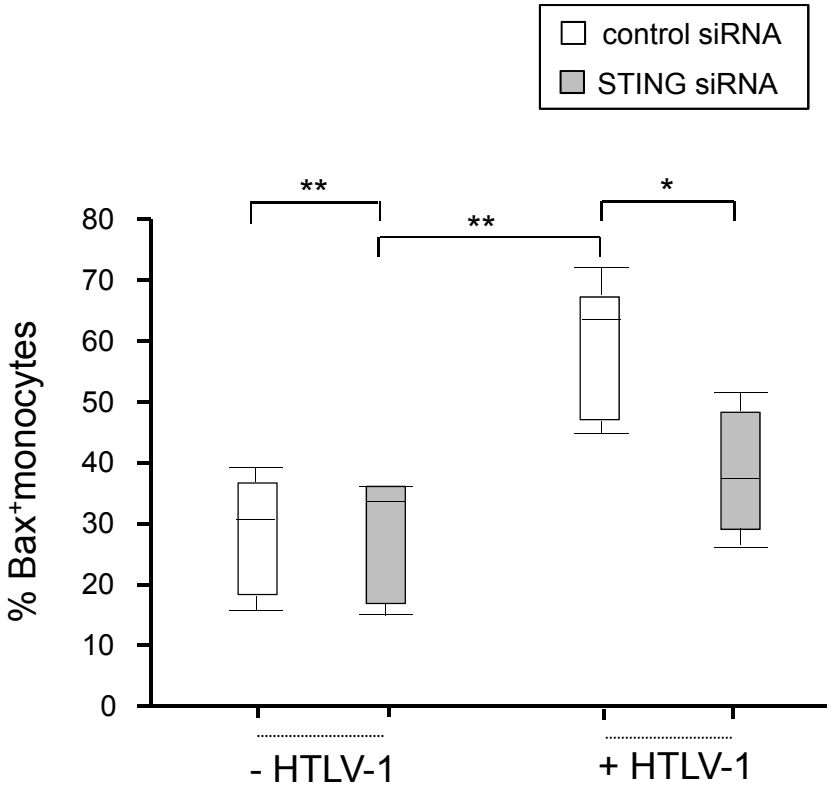
control siRNA
STING siRNA
**
**
*
% Bax+monocytes
80
70
60
50
40
30
20
10
0
- HTLV-1
+ HTLV-1

Figure S7

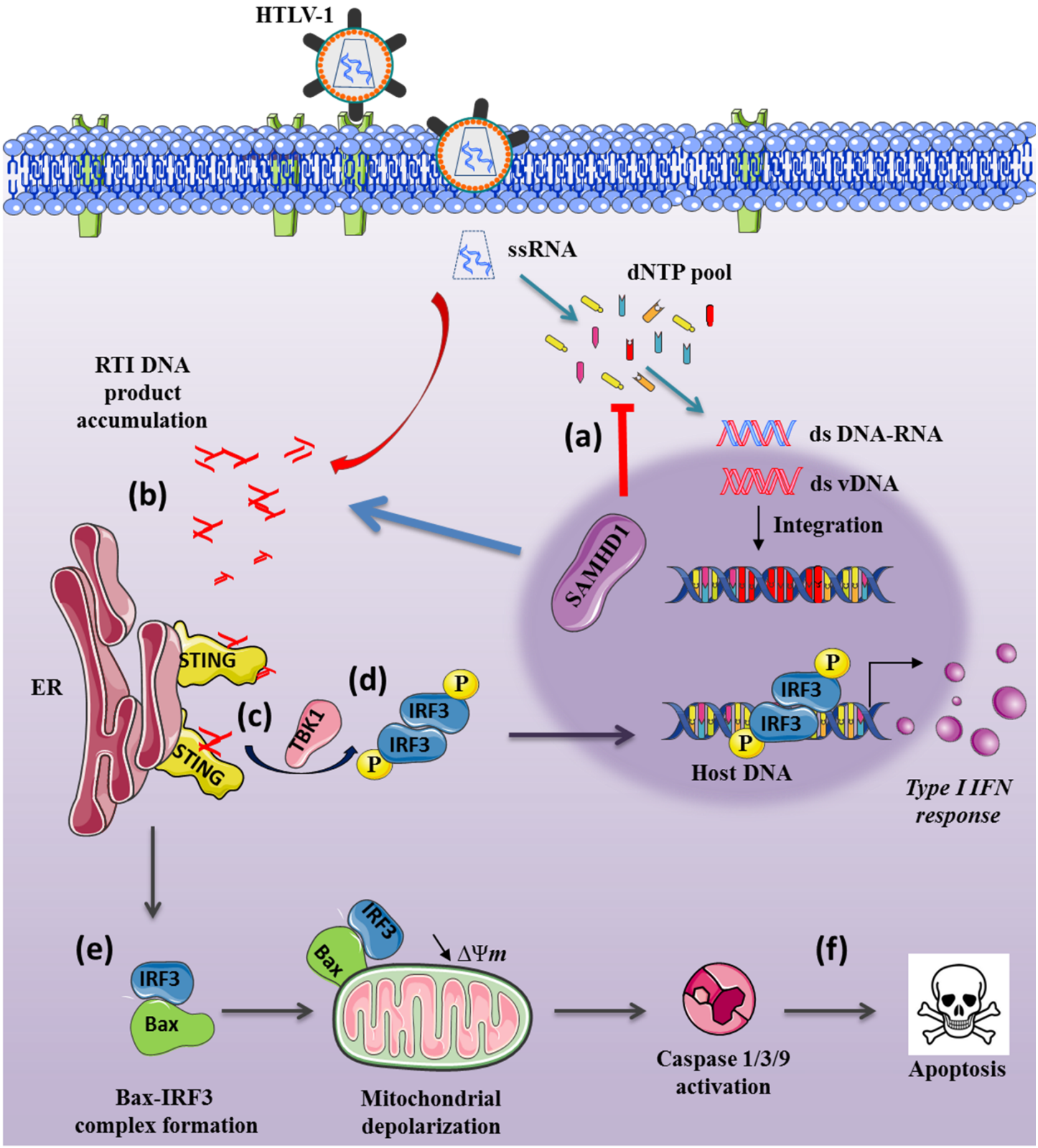
HTLV-1
ssRNA
dNTP pool
RTI DNA product accumulation
(a)
ds DNA-RNA
ds vDNA
Integration
(b)
SAMHD1
ER
STING
STING
(c)
TBK1
(d)
P
IRF3
IRF3
P
P
IRF3
IRF3
P
Host DNA
Type I IFN response
(e)
IRF3
Bax
Bax-IRF3 complex formation
IRF3
Bax
ΔΨm
Mitochondrial depolarization
(f)
Caspase 1/3/9 activation
Apoptosis

EXPERIMENTAL PROCEDURES

Products

RPMI-1640 media, FBS and antibiotics were provided by Wisent Technologies (CA, USA). All monoclonal antibodies (mAbs) and products used for flow cytometry were purchased from Biolegend (CA, USA), except for anti-cleaved caspase 3-PE mAbs, Annexin-V buffer 10X and Annexin-V-V450 obtained from Becton Dickinson (NJ, USA). Anti-p19 mAbs (clone TP-7) was purchased from ZeptoMetrix Corporation (NY, USA), whereas anti-gp46 mAbs (clone 67/5.5.13.1) was purchased from Abcam (MA, USA). Anti-Tax-FITC mAbs (clone LT4) was generously provided by Dr. Yuetsu Tanaka (Kitasato University, Kanagawa, Japan). All antibodies included in western blotting analyses came from Cell signaling Biotechnology Inc. (MA, USA), except for anti-Bax mAbs (Santa Cruz Biotechnology Inc.; TX, USA). Pan-caspase inhibitor Z-VAD-FMK (ZVAD) was purchased from R and D Systems^{R} (MN, USA). All cell lines were obtained from the ATCC^{TM} (VA, USA).

Purification of monocytes

Leukaphereses from healthy donors were obtained from the Royal Victoria Hospital, Montreal (QC, Canada), with informed consent of the patients and in agreement with the Royal Victoria Hospital, the Jewish General Hospital, and McGill University Research Ethics Committee. PBMCs were isolated using Ficoll-Hypaque gradient (GE Healthcare BioScience Inc., Ontario, Canada). Monocytes were purified from PBMCs using the untouched monocyte isolation kit (EasySep® Human Monocyte Enrichment Kit without CD16 Depletion; StemCell Technologies, Vancouver, BC, Canada), allowing for more than 94% purification without any cell stimulation and apoptosis.

HTLV-1 purification and *in vitro* infection

HTLV-1 viruses were purified from MT-2 supernatants. Cells were seeded overnight in complete RPMI (2.10^6 cells/mL). Supernatants were collected and ultra-centrifuged for 2h at 30,000 g at 4ºC. The viral pellet was re-suspended in complete RPMI, and HTLV-1 particles were quantified by gag p19 ELISA assays (ZeptoMetrix). 200,000 purified monocytes were incubated with 2µg HTLV-1 for 3h at 37ºC in 0.5 mL RPMI complete with or without 100µM Z-VAD-FMK. To specifically block HTLV-1 infection, neutralizing anti-gp46 mAbs (at 10µg/mL; Abcam) were incubated 30 minutes at 4ºC with HTLV-1 prior *in vitro* infection. At 3h pi, monocytes were washed twice in complete RPMI and then co-cultured with 8.10^5 autologous monocyte-depleted PBMCs (1 ml complete RPMI; [HTLV-1] = 2µg/mL).

HTLV-1 DNA quantitation and nuclear extraction

$2\text{-}4.10^6$ monocytes, isolated using magnetic beads and infected or not with HTLV-1, were collected at several time points (3-120h pi), and washed with PBS. Cells were pelleted and stored at -80ºC, prior to various DNA extraction protocols. *Whole cell DNA:* DNA was extracted from stored pellets using the DNeasy® Blood & Tissue kit (Cat. Number: 69504; Qiagen Inc.) using the manufacturer's instructions. *Nuclear DNA:* nuclear material was extracted from stored pellets; cells were lysed in 10mM Tris (pH 7.9), 10mM KCl, 0.1mM EDTA, and 0.1mM EGTA, for 15 minutes. NP40 was then added and the lysates were centrifuged 3 minutes at 13,000 rpm to obtain a nuclear pellet that was used for subsequent DNA extraction (Qiagen). *ALU PCR:* integrated HTLV-1 DNA was amplified from purified nuclear DNA as previously described (Liszewski et al., 2009), with the following modifications. Cloned Pfu DNA polymerase (Cat. Number:

B0093; Bio Basic) was used, and the primer sequences for Alu (forward) and gag (reverse) are listed in **Table S1**. HTLV-1 DNA load was determined on total or nuclear cell extract, or ALU PCR products, using the real-time SYBR green PCR method. The assay was analyzed using the AB 7500 real-time PCR system (Applied Biosystems, CA, USA) with PerfeCTa® SYBR® Green FastMix® (Cat. Number: 95074; Quanta Biosciences, MD, USA) using ~200ng of extracted DNA, or 0.1µl of amplified integrated DNA. The endogenous erv-3 gene was used to normalize the amount of DNA per reaction. The real-time PCR conditions were: 95°C for 10 minutes, and 45 cycles of 95°C for 15 seconds followed by 60°C for 1 minute.

Measurement of viral genomic RNA

Following HTLV-1 infection, 4.10^6 isolated monocytes were incubated 6 minutes with 0.25% trypsin at 37ºC to remove non-internalized HTLV-1 particles and washed twice in PBS. Cells were thereafter pelleted and stored at -80ºC in RLT buffer in the presence of β-mercaptoethanol for further use. Total RNA was extracted using RNeasy kit (Qiagen Inc.) according to the manufacturer's instructions. The RNA integrity and purity was assessed with the Thermo Scientific NanoDrop 1000 (Thermo Scientific, DE, USA). Complementary DNA (cDNA) was then produced by reverse transcription using the Applied Biosystems High Capacity cDNA Reverse Transcription Kit (Qiagen Inc.). The subsequent real-time PCR parameters were described in the previous section, except for the fact that β-actin was used as the housekeeping gene.

Flow cytometry

At several time pi, collected cells were incubated for 10 minutes at 4ºC in PBS + 10% FBS to avoid any unspecific binding. *Measurement of viral infection:* Cells were then

stained for 10 minutes at 4ºC with anti-CD14-APC H7, anti-CD3-PE Cy7 in PBS. Cells were washed twice and fixed at room temperature (RT) in BD FACS Lysing Buffer (Becton Dickinson) and incubated with anti-Tax-FITC and anti-p19-Alexa 647 mAbs for 20 minutes at RT in 0.25% saponin. Anti-p19 IgG_1 antibody was conjugated to Alexa647 dye using the Zenon^R mouse IgG_1 labeling kit (number: Z25008; Life Technologies Inc., ON, USA) according to the manufacturer's protocol. After three final washes in PBS, we collected approximately 20,000 gated events on the BD Fortessa flow cytometer (Becton Dickinson) and analyzed the data using the DIVA software. *Apoptosis assay:* To assess apoptosis, cells were washed and labeled for 10 minutes at 4ºC with anti-CD14-APC H7, anti-CD3-PE Cy7 and Annexin-V-V450 in calcium buffer 1X (Becton Dickinson). ICS of $_{CL}$caspase-3 or Bax was the same as mentioned below for HTLV-1 antigens, except for the fact that all solutions were diluted in calcium buffer. *Mitochondria depolarisation:* This was evaluated through measurement of the loss of retention of the cationic fluorescent dye $DiOC_6(3)$ (used at 10nM), as previously described(Kalbacova et al., 2003). $DiOC_6(3)$-related fluorescence was finally analyzed on $CD3^-CD14^+$monocytes by flow cytometry.

Western blotting

Protein lysates (2-10 μg) from monocytes were subjected to Western blot analysis as previously described (Oliere et al., 2010).

Small interfering RNA assays

10^7 purified monocytes were electroporated in the presence of control or specific siRNA using Nucleofactor II technology according the manufacturer's protocol (Amaxa human monocyte nucleofactor kit). SAMHD1-, STING-, RIG-I- or Bax-specific siRNA as well

as siRNA-A negative control were obtained from Santa Cruz Biotechnology (Cat. numb. sc-76442, sc-92042, sc-61480, sc-29212, and sc-37007 respectively; CA, USA). 300nM siRNA was transfected per condition in RPMI + 30% FBS overnight without antibiotics. Transfected monocytes were washed at 1500 rpm for 5 minutes to remove necrotic cells and cultured with autologous PBMC. For SAMHD1 and STING siRNA treatments, monocytes were washed and counted for further *in vitro* HTLV-1 infection 3 days post-transfection. RIG-I and Bax siRNA treated monocytes were similarly processed 3h post-transfection.

Biotinylated retroviral DNA_{90} assay

Retroviral DNA was produced by Integrated DNA technologies (IA, USA). HTLV-1 $ssDNA_{90}$ is the reverse complement of the 5'utr region (315-404 of complete HTLV-1 genome; NCBI) that is 90 bases long and conjugated with biotin on the 5' end. The sequence is: 5'-CTG TGT ACT AAA TTT CTC TCC TGG AGA GTG CTA TAG AAT GGG CTG TCG CTG GCT CCG AGC CAG CAG AGT TGC CGG TAC TTG GCC GTG GGC-3'. HTLV-1 biotinylated ssDNA-sense strand was annealed to the reverse complement to create $dsDNA_{90}$. As a negative control, we used an scrambled RTI (generated by randomizing the U5 sequence; 5'-ATT CAG CTC ACG GCG TCG AGT GCT GCT CGA TGG CTC CTT AGT CCT GCT AAG TCG AGG TGG CTA ATC CGG TAG TCG GTC GGA TGG AAT TCG-3'). HIV-1 $ssDNA_{90}$ is also the biotinylated reverse complement of the 5'utr region (97-186 of complete HIV-1 genome; NCBI). The sequence is: 5'-CGC CAC TGC TAG AGA TTT TCC ACA CTG ACT AAA AGG GTC TGA GGG ATC TCT AGT TAC CAG AGT CAC ACA ACA GAC GGG CAC ACA CTA CTT-3'. 10^7 monocytes were transfected with 10µg $vDNA_{90}$ for 24h in RPMI +

30% FBS in the absence of antibiotics. Monocytes were washed and then co-cultured in complete RPMI with $CD14^{neg}$PBMCs.

STING pull-down and Bax co-immunoprecipitation

Monocytes were infected with HTLV1 or transfected with biotinylated RTI for 6h (pull-down) or 3h (co-IP). Monocytes were lysed using CHAPS buffer with protease inhibitors as previously described (Samuel et al., 2010). 3µg protein was collected and referred to as the "input" fraction. *STING Pull-down:* ~200µg protein was incubated with 20µl streptavidin bead resin (Thermo Scientific) overnight at 4ºC while rotating. Bead-protein complexes were washed 6 times in CHAPS buffer and then incubated 10 minutes at 100ºC with 2X loading dye. Lysates were centrifuged 3 minutes at 13,000 rpm to remove the beads and subjected for western blotting analyses. *Anti-Bax co-IP:* Protein L-agarose beads (Santa Cruz Inc.; sc-2336) were washed with 0.2 mol/L triethanolamine pH 9.0. 30µg of anti-Bax mAbs was cross-linked to 300µL of L-agarose beads in the presence of dimethylpentylamine-Hcl for 1h at RT. After washes in triethanolamine, 2µg of cross-linked anti-Bax beads was incubated overnight with ~200µg protein in 1% CHAPS lysis buffer at 4ºC overnight while rotating. Immunoprecipitates were collected, washed 5 times in CHAPS buffer and then incubated 10 minutes at 100ºC with 1X loading dye. Samples were centrifuged and subjected to western blotting analyses.

Statistical analysis

Statistical analyses were performed using the non-parametric Mann-Whitney *U* test, assuming independent samples. However, differences among the treatment groups performed with n = 3 samples were analyzed by the parametric unpaired Student *t* test. *P*

values of less than 0.05 were considered statistically significant. ***, $P < 0.001$; **, $P < 0.01$ and *, $P < 0.05$.